

# Paleomagnetism of the Teel basalts from the Zavkhan terrane: Implications for Paleozoic paleogeography in Mongolia and the growth of continental crust

T.M. Kilian<sup>1,\*</sup>, N.L. Swanson-Hysell<sup>1</sup>, U. Bold<sup>2</sup>, J. Crowley<sup>3</sup>, and F.A. Macdonald<sup>2</sup>

<sup>1</sup>DEPARTMENT OF EARTH AND PLANETARY SCIENCE, UNIVERSITY OF CALIFORNIA, BERKELEY, CALIFORNIA 94720, USA

<sup>2</sup>DEPARTMENT OF EARTH AND PLANETARY SCIENCES, HARVARD UNIVERSITY, CAMBRIDGE, MASSACHUSETTS 02138, USA

<sup>3</sup>DEPARTMENT OF GEOSCIENCES, BOISE STATE UNIVERSITY, BOISE, IDAHO 83725, USA

## ABSTRACT

A narrow extensional basin on the Zavkhan terrane of Mongolia exposes a >1.8-km-thick succession of basalt flows within the Teel Formation, along with rhyolites and interflow sediments. We present new U-Pb zircon ages of  $446.03 \pm 0.21$  Ma (chemical abrasion–isotope dilution–thermal ionization mass spectrometry) on a rhyolite in the Teel Formation and  $286 \pm 5$  Ma (laser ablation–inductively coupled plasma–mass spectrometry) on a nearby granitic intrusion (Tonkhil Complex). New paleomagnetic data yield a magnetite remanence that is likely primary, acquired during cooling of flows. The mean direction is statistically improved after tilt corrections; however, the tilt test significance is limited given the low variation in tilt between flows. We interpret a second remanence, held by hematite, as an overprint that was likely acquired in the Paleozoic Era. The tilt-corrected magnetite direction implies a paleolatitude of  $\sim 20^\circ$ , while the hematite overprint is equatorial in both geographic and tilt-corrected coordinates. The ca. 446 Ma Teel remanence is consistent with an Ordovician paleogeographic position near Siberia; however, the hematite direction requires subsequent drift to the equator, indicating that these Mongolian terranes were not continuously connected to Siberia, which moved away from the tropics during the Paleozoic Era. This result is consistent with biogeographic constraints and a previously proposed model wherein Amuria traveled with North China during the Permian Period and collided with Siberia during the Jurassic to Triassic closure of the Mongol-Okhotsk Ocean. In this model, continental growth occurred through the collision and oroclinal buckling of a ribbon continent rather than long-lived accretion on the margin of a major craton.

LITHOSPHERE

GSA Data Repository Item 2016284

doi: 10.1130/L522.1

## INTRODUCTION

The  $\sim 5000$ -km-long Central Asian orogenic belt (Fig. 1) is considered the largest area of Phanerozoic crustal growth preserved in the geological record, and yet, the tectonic history and geological context of terrane assembly remain controversial and underconstrained (e.g., Khain et al., 2003; Kröner et al., 2010; Mossakovsky et al., 1994; Şengör and Natal'in, 1996; Şengör et al., 1993; Wilhem et al., 2012; Windley et al., 2007; Yakubchuk, 2008). Detailed geological mapping for vast regions of the Central Asian orogenic belt and the generation of more precise geochronological constraints and Paleozoic paleomagnetic poles are necessary to constrain the history of terrane assembly. Here, we provide new Paleozoic geological, geochronological, and paleomagnetic constraints on the Zavkhan terrane of Mongolia and compare the implied


paleolatitudes to those of the major cratons that border the Central Asian orogenic belt—Siberia and North China (Fig. 1). These data provide new insight into the paleogeographic history of the Zavkhan terrane and conjoined terranes (grouped as “Amuria” in Van der Voo et al., 2015; Fig. 1).

Paleomagnetic data from the Siberia and North China cratons provide constraints on the closure of the Mongol-Okhotsk Ocean, which constituted the final stages of crustal amalgamation within the Central Asian orogenic belt (Cogné et al., 2005; Van der Voo et al., 2015). These data track the convergence of Siberia and North China through the Jurassic Period and amalgamation by the earliest Cretaceous Period (Cogné et al., 2005; Van der Voo et al., 2015). In the model of Van der Voo et al. (2015), this closure is associated with an arc-system that folded in on itself, leading to a scissor-like collision between Siberia and North China. This reconstruction reconciles the history of paleolatitudinal convergence, tomographic evidence for a slab below Siberia, and the interpretation that the

Mongol-Okhotsk Ocean terminated at the Tuva-Mongolia orocline (Van der Voo et al., 2015). In the models of Cogné et al. (2005) and Van der Voo et al. (2015), Amuria is purportedly associated with North China, while terranes north of the proposed Mongol-Okhotsk Ocean suture are interpreted to have been associated with Siberia. These models also allow the Mongolian terranes to be connected along the western margin of the Mongol-Okhotsk Ocean, effectively connected with both Siberia and North China during the Mesozoic Era. But how far back in time can we connect Mongolian terranes to Siberia and/or North China?

Biogeographic constraints link many of the Mongolian terranes with Siberia during the early Paleozoic Era, and some (Cocks and Torsvik, 2007) have extended that connection to the present by maintaining a peri-Siberian location for Mongolian terranes since the Ordovician Period. Paleomagnetic constraints indicate far different paleolatitudes for North China and Siberia until the Permian Period (Kravchinsky et al.,

\*E-mail: taylor.kilian1@gmail.com

Taylor Kilian  <http://orcid.org/0000-0001-7859-293X>

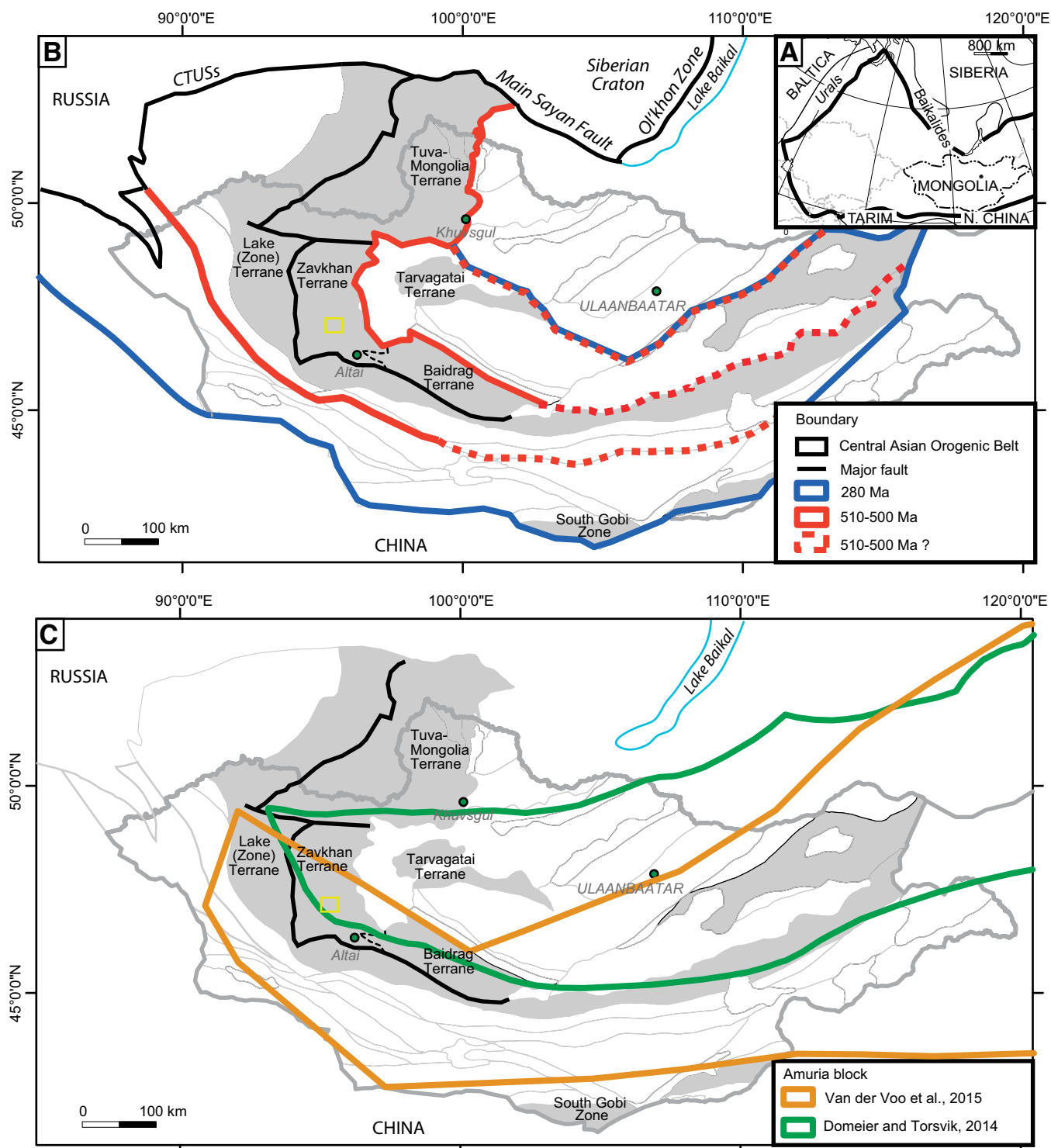


**Figure 1.** (A) Outline of the Central Asian orogenic belt shown with the Siberia craton to the north and the Tarim and North China cratons to the south (modified from Şengör and Natal'in, 1996). (B) Simplified terrane map of Mongolia (Badarch et al., 2002) with boundaries extending into Russia. Regions shaded gray are areas containing Precambrian basement. The terrane grouping shown is based on that proposed by Bold et al. (2016) and is informed by new geochronology and comparative tectonostratigraphy. Positions of the Charysh-Terekta-Ulagan-Sayan suture-shear zone (CTUSs), Main Sayan fault, and Ol'Khon zone are after Glorie et al. (2011) and Buslov (2011). (C) Outline of Amuria, as implemented in the paleogeography reconstructions of Domeier and Torsvik (2014) (and used in reconstructions of Van der Voo et al., 2015), along with the outline of Amuria proposed by Van der Voo et al. (2015), in which the northern boundary is interpreted as the suture resulting from closure of the Mongol-Okhotsk Ocean. The small yellow box within the Zavkhan terrane shows the region displayed in the Figure 2 geologic map.

2002). Consequently, it has remained unclear how the Mongol-Okhotsk Ocean formed and where the fringing (Mongolian) terranes, such as the Zavkhan terrane, originated.

The Zavkhan terrane is a Precambrian cratonic fragment that is mantled with Neoproterozoic and early Paleozoic sedimentary successions and embedded in the Central Asian orogenic belt (Fig. 1). New geochronologic data from the Zavkhan terrane in conjunction with geologic mapping (Bold et al., 2016) lead to the terrane grouping shown in Figure 1B. The ca. 510–500 Ma outline shows the terrane association we interpret to have existed following the late Ediacaran to Early Cambrian collision of the Zavkhan and Tuva-Mongolia terranes (Tuva-Mongolia massif of Kuzmichev et al., 2001; Tuva-Mongolian microcontinent of Windley et al., 2007) with the Baidrag and Lake terranes (Fig. 1B). Note that distinct differences in the tectonostratigraphy of the Zavkhan and Tuva-Mongolia terranes in comparison to the Baidrag and Lake terranes are inconsistent with their association prior to the late Ediacaran Period (Bold et al., 2016). Tectonic and paleogeographic syntheses have previously referred to various groupings of the terranes in central and southeastern Mongolia as the Central Mongolia (e.g., Ilyin, 1990) or the Amuria block (e.g., Van der Voo et al., 2015). The outlines of Amuria used in recent reconstructions (e.g., Domeier and Torsvik, 2014) and that proposed by Van der Voo et al. (2015), who interpreted it to have collided with Siberia and peri-Siberian terranes, are shown for reference in Figure 1C. Our preferred terrane grouping significantly extends northward the boundary of terranes that we consider to have been part of Amuria. There is a strong tectonostratigraphic basis for this grouping (Bold et al., 2016). Such a terrane outline is consistent with the model of Van der Voo et al. (2015), where subduction of the Mongol-Okhotsk Ocean became doubly vergent and resulted in oroclinal bending of the terranes on the northern margin of Amuria. However, this modification reassigns some of the peri-Siberian crustal material of Van der Voo et al. (2015) (i.e., terranes assumed to be on the northern margin of the Mongol-Okhotsk Ocean) and interprets them as having a shared history with Amuria, namely, Tuva-Mongolia. Note that the Amuria outline we use within paleogeographic reconstructions (outline shown in Fig. 1) marks the current geography, but that there was Paleozoic to Mesozoic oroclinal bending within Amuria between the Tuva-Mongolia, Zavkhan, and Baidrag terranes.

Constraining the mechanisms of crustal growth associated with the Central Asian orogenic belt necessitates an understanding of the

origin of crust within the orogeny, as well as constraints on when and where collision and accretionary events occurred. The origin and the tectonic history of the Tuva-Mongolia, Zavkhan, Baidrag, and Lake terranes (Fig. 1) are currently underconstrained. Of particular interest is whether or not these terranes were in close proximity to Siberia or other landmasses, such as North China, during the Paleozoic Era. Şengör et al. (1993) proposed that these Mongolian terranes had a close association with Baltica and Siberia as a Proterozoic continental arc, which separated from the cratonic margin via back-arc extension during Ediacaran to Cambrian times. In this model, the distended peri-Siberian arc, referred to as the Kipchak arc, was oroclinally buckled during the Devonian Period (Şengör et al., 1993; Şengör and Natal'in, 1996), and Amuria protruded south (present coordinates) as a peninsula through the Permian Period. A Siberian origin of the Tuva-Mongolia, Zavkhan, Baidrag, and Lake terranes was also favored by Cocks and Torsvik (2007), Khain et al. (2003), Kuzmichev et al. (2001), Yakubchuk (2008), Kovalenko (2010), and Wilhem et al. (2012). Generally, in these models, the Mongolian terranes are thought to be underlain by Siberian crust and to have occupied a Neoproterozoic to Paleozoic arc to extensional back-arc system on the margin of Siberia that closed and reopened multiple times during and between episodes of accretion.

Other studies have argued that the Tuva-Mongolia, Zavkhan, Baidrag, and Lake terranes may be Gondwana-derived fragments that accreted to Siberia—these interpretations are based on paleomagnetic data from the Neoproterozoic Zavkhan Formation (e.g., Levashova et al., 2010) and Paleozoic detrital zircon provenance data (e.g., Rojas-Agramonte et al., 2011). Paleontological data suggest that some of these Mongolian terranes had a close association with Siberia or “peri-Siberian” terranes during the Cambrian and Silurian Periods (e.g., Cocks and Torsvik, 2007); however, it remains unclear if these terranes were near Siberia during later Paleozoic time (for a more complete review of Neoproterozoic to early Paleozoic tectonic models of Mongolia, see Bold et al., 2016). Driven by paleomagnetic and tomographic data, recent studies have suggested that the Mongolian terranes grouped with Amuria (Fig. 1) remained separate from Siberia and traveled with North China until the Jurassic Period (Edel et al., 2014; Van der Voo et al., 2015). Here, we use new paleomagnetic data from the Zavkhan terrane and compile existing paleomagnetic data from the adjacent terranes to develop a refined Paleozoic paleogeographic model of Mongolian terranes now embedded within the Central Asian orogenic belt.

## GEOLOGIC SETTING OF THE TEEL FORMATION

The Neoproterozoic volcanic and sedimentary rocks of the Zavkhan terrane were buried by ~1.5 km of Early Cambrian foreland basin deposits and then deformed and metamorphosed during subsequent Paleozoic orogenesis (Bold et al., 2016). After late Ediacaran to Ordovician accretion of arc terranes to the south of the Zavkhan terrane (Jian et al., 2014; Macdonald et al., 2009), the Ordovician to Silurian record of the Mongolian terranes is marked by sinistral transtension, extensional magmatism, and basin formation (e.g., Gibson et al., 2013; Kröner et al., 2010; Lamb and Badarch, 2001).

In our study area within the Zavkhan terrane (Fig. 2), Ordovician to Silurian transtension resulted in narrow rift basins that accommodated volcanic and minor sedimentary rocks of the Teel Formation. The Teel Formation is composed of bimodal series of rhyolite and basalt with intervals of siliciclastic sedimentary rocks (Togtokh et al., 1995). In the Khukh Davaa region, more than 1.8 km of basalt, rhyolite, and siliciclastic sedimentary rocks of the Teel Formation were erupted and deposited (Fig. 2). The stratigraphy is dominated by basaltic lava flows that texturally vary from aphyric to plagioclase porphyritic to ophitic, with variable amounts of secondary oxidation (Fig. 3). The excellent preservation of some of the basalt flows and their iron oxides, such as in the ophitic Z31 flow (Figs. 3A and 3B), suggests that alteration, where present, is associated with localized hydrothermal fluid flow rather than regional metamorphism. This oxidation results in variably present hematite, which is apparent on the macroscopic scale as Liesegang banding and on the microscopic scale as hematite staining and replacement near and within iron-oxide and iron-silicate grains (Figs. 3D–3H). Felsic eruptive centers are preserved approximately halfway through the stratigraphy (Fig. 2). Interbedded red beds were previously mapped as the Devonian Tsagaanshoroot Formation, which was paleontologically dated in the Lake terrane (Togtokh et al., 1995). New U-Pb geochronologic data from a Teel Formation rhyolite within the succession (Figs. 2 and 4) in conjunction with measured stratigraphic sections demonstrate that at least some of these sedimentary rocks on the Zavkhan terrane are associated with the Ordovician to Silurian Teel Formation.

The Zavkhan and neighboring terranes were intruded by Permian granitic plutons. On the Zavkhan terrane, these plutons are mapped as the Tonkhil Complex, but U-Pb zircon geochronology has not been previously presented in support of this age assignment. The Tonkhil

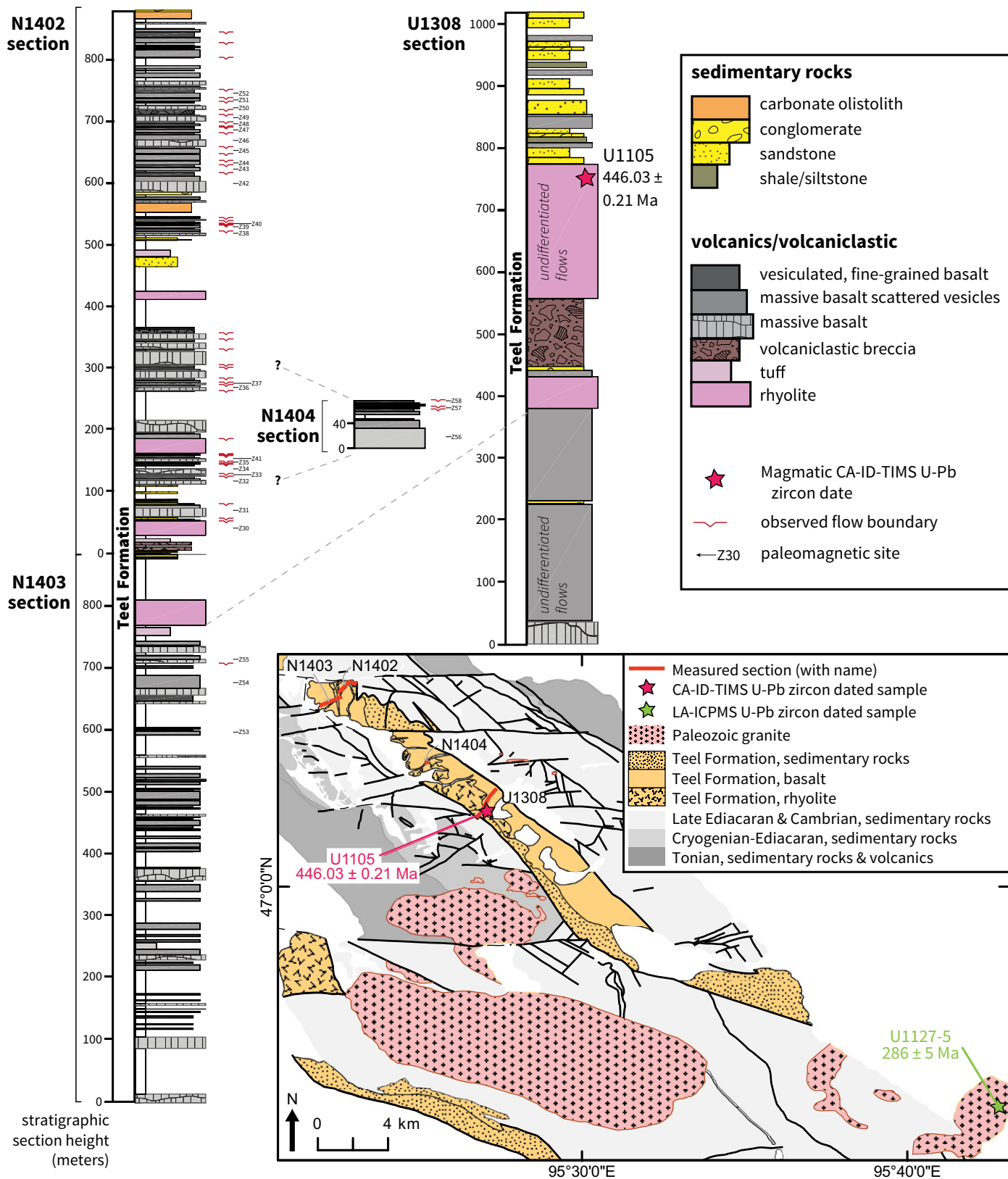


**Figure 2.** Stratigraphic sections through the Teel Formation showing the positions of flow boundaries and paleomagnetic sites. As seen in the inset geological map, the small extensional basin hosting the Teel Formation formed within Neoproterozoic sedimentary rocks and is proximal to subsequent plutonism. The locations of measured sections and dated samples are shown on the map. CA-ID-TIMS—chemical abrasion–isotope dilution–thermal ionization mass spectrometry; LA-ICP-MS—laser ablation–inductively coupled plasma–mass spectrometry.

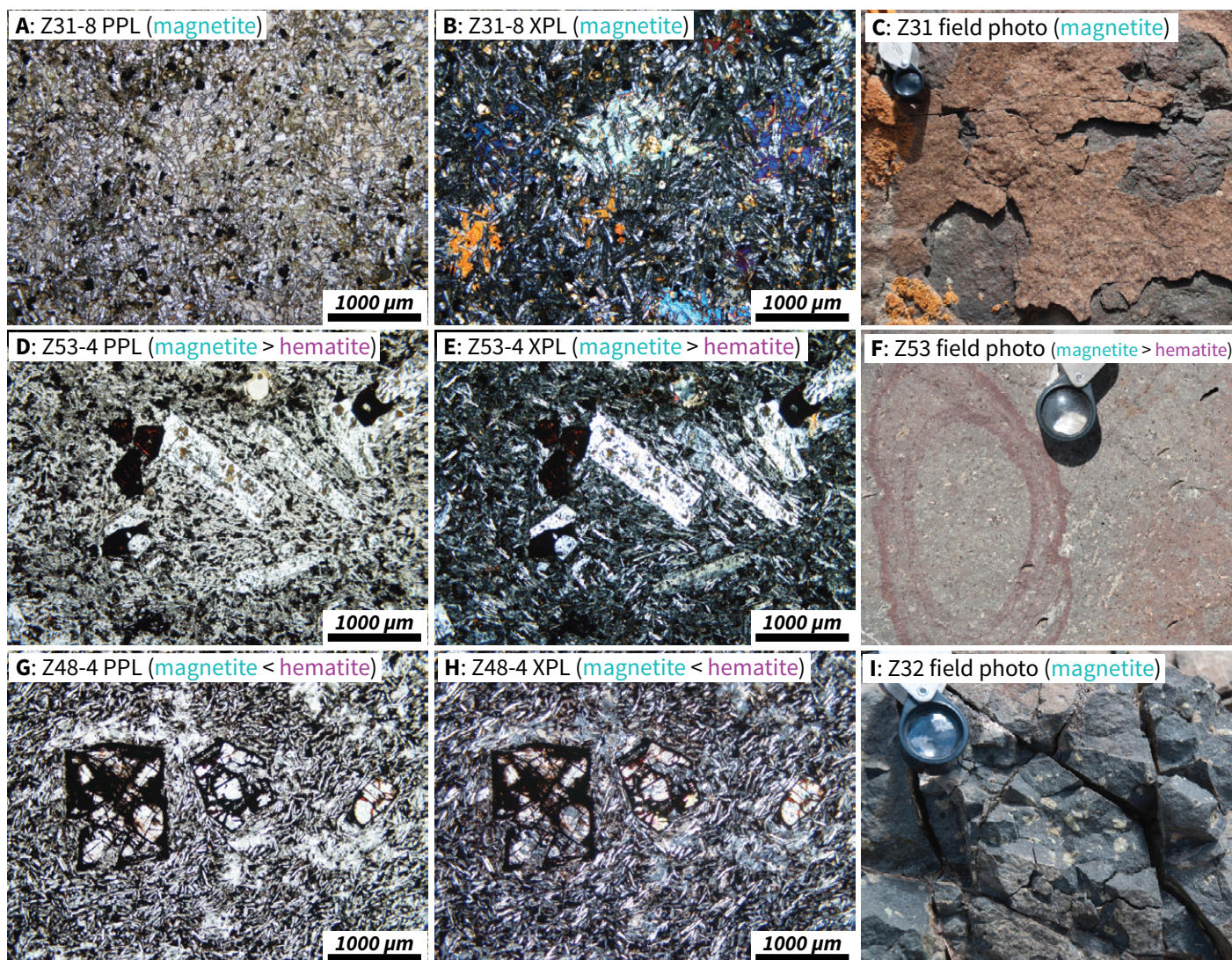


**Figure 3.** (A–I) Petrographic and field photos of Teel Formation basaltic lava flows. (A–B) Sample Z31-8 has remanence dominated by magnetite with no indication of hematite (Fig. 5A). The basalt has an ophitic texture with very well-preserved augite oikocrysts. (A) Thin section under plane-polarized light (PPL) and (B) same thin section under cross-polarized light (XPL). (C) The outer weathered surface of the Z31 lava flow shows the ophitic texture and breaks away to reveal fresher basalt underneath. Glass within the hand lens, shown for scale in the field photographs, is 1.8 cm across (C, F, I). (D–E) Sample Z53-4 has a remanence that is dominated by magnetite with some hematite (Fig. 5C). There is hematite staining apparent in the vicinity of Fe-Ti-oxide grains in the photomicrographs. (F) The sample comes from the plagioclase-phyric Z53 flow in which there is large-scale hematite Liesegang banding indicating spatially variably oxidation. (G, H) Sample Z48-4 has a remanence that is dominated by hematite with minor magnetite that holds onto the same magnetite direction seen in the less-altered flows (Fig. 5D). In this sample, altered clinopyroxene phenocrysts are rimmed and crosscut by hematite, and there is hematite in the groundmass. (I) Field photo of the plagioclase-phyric Z32 flow, which is well preserved and has a remanence that is solely held by magnetite.

Complex granites are alkaline and characterized by coarse crystalline syenite-porphry. The widespread nature of these plutons across the Precambrian cratonic fragments (e.g., Byamba, 2009; Jahn et al., 2009; Kröner et al., 2010; Yarmolyuk et al., 1999; Zacek et al., 2016) supports the interpretation that the regions on both sides of the Mongol-Okhotsk Ocean originally formed a continuous arc that was later oroclinally buckled. The proximity of some of these intrusions to the studied Teel Formation sections

(Fig. 2) has the potential to have influenced the paleomagnetic remanence of the basalts and may have resulted in oxidation in some of the samples that can be seen petrographically (Fig. 3).

#### U-Pb GEOCHRONOLOGY METHODS AND RESULTS

A sample of Teel Formation rhyolite (U1105) was collected in the Khukh Davaa region in

stratigraphic section U1308 (Fig. 2; 47.0387°N, 95.4504°E). A granite from the Permian Tonkhil Complex (U1127-5) was sampled in the same region at the opening of the Salaa Gorge (Fig. 2; 46.8786°N, 95.7105°E). Zircons from the samples were first analyzed by laser-ablation–inductively coupled plasma–mass spectrometry (LA-ICP-MS), and grains of sample U1105 were analyzed by chemical abrasion–isotope dilution–thermal ionization mass spectrometry (CA-ID-TIMS) at Boise State University.

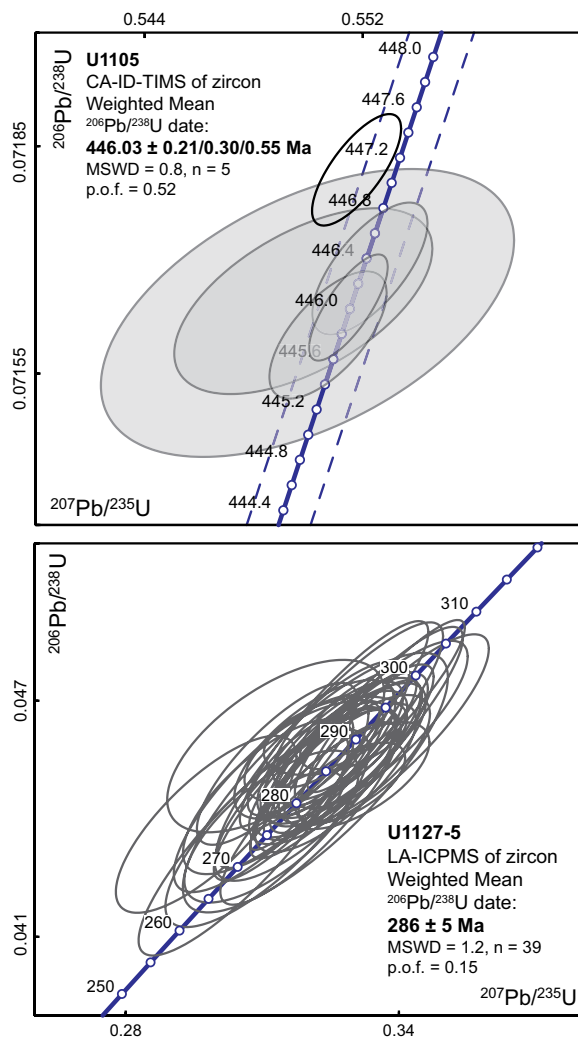


**Figure 4. Concordia diagrams of samples dated in this study. (A) U1105 is a Teel Formation rhyolite that was dated by the chemical abrasion–isotope dilution–thermal ionization mass spectrometry (CA-ID-TIMS) method. The weighted-mean date was calculated from five analyses (shaded ellipses) with one excluded analysis (open ellipse). U1127-5 is a granitic pluton of the Tonkhil Complex dated by the laser ablation–inductively coupled plasma–mass spectrometry (LA-ICP-MS) method. The weighted mean was calculated from 39 analyses. MSWD—mean square of weighted deviates; p.o.f.—probability of fit.**

## Methods

Zircon grains were separated following the protocol outlined in Bold et al. (2016) and Macdonald et al. (2014). The grains were analyzed by LA-ICP-MS using a ThermoElectron X-Series II quadrupole ICPMS and New Wave Research UP-213 Nd:YAG ultraviolet (213 nm) laser-ablation system. In-house analytical protocols, standard materials, and data reduction software were used for acquisition and calibration of U–Pb dates and a suite of high field strength elements (HFSE) and rare earth elements (REE). A weighted-mean date was calculated using Isoplot 4.15 (Ludwig, 2008) from errors on individual dates that do not include the standard calibration uncertainties. However, the error on the date includes the standard calibration uncertainty within the experiment and is given at  $2\sigma$ .

Zircon grains from sample U1105 were removed from epoxy mounts after LA-ICP-MS and subjected to a modified version of the

CA-ID-TIMS method of Mattinson (2005), with analyses conducted on single grains. Details of the analytical techniques are described in Bold et al. (2016). All common Pb in analyses was attributed to laboratory blanks and subtracted based on the measured laboratory Pb isotopic composition and associated uncertainty. The weighted-mean  $^{206}\text{Pb}/^{238}\text{U}$  date was calculated from equivalent dates and plotted using Isoplot 4.15 (Ludwig, 2008). The error is given at  $2\sigma$  and reported as  $\pm x/y/z$ , where  $x$  is the internal error based on analytical uncertainties only, including counting statistics, subtraction of tracer solution, and blank and initial common Pb subtraction;  $y$  includes systematic uncertainty associated with tracer calibration; and  $z$  additionally includes systematic uncertainty associated with the  $^{238}\text{U}$  decay constant. When comparing these dates with those from other U–Pb laboratories not using the EARTHTIME tracer,  $\pm y$  should be used. Comparisons with other chronometers should utilize  $\pm z$ .

## Results

Five of the six zircon grains from the Teel Formation rhyolite (U1105) yielded equivalent CA-ID-TIMS  $^{206}\text{Pb}/^{238}\text{U}$  dates with a weighted mean of  $446.03 \pm 0.21/0.30/0.55$  Ma (mean square of weighted deviates [MSWD] = 0.8, probability of fit = 0.52; Table 1; Fig. 4). This date is the interpreted magmatic age. One date is slightly older and interpreted to reflect the presence of an inherited component.

Thirty-nine of the 42 zircon grains from the granite pluton (U1127-5) yielded equivalent LA-ICP-MS  $^{206}\text{Pb}/^{238}\text{U}$  dates with a weighted mean of  $285 \pm 5$  Ma (MSWD = 1.2, probability of fit = 0.15; Table 2; Fig. 4). This date is interpreted as the magmatic age.

## PALEOMAGNETISM METHODS AND RESULTS

During a field season in 2014, we sampled 28 lava flows from the Teel Formation with the goal of developing a paleomagnetic pole to constrain the position of the Zavkhan terrane in the Late Ordovician Epoch. All samples were collected within the context of volcanostratigraphic sections (Fig. 2). Cores were obtained with a gas-powered drill and oriented using a Pomeroy orienting device. Whenever possible, sun compass measurements were taken in addition to magnetic orientations and were used preferentially to constrain sample orientation. Each individual lava flow sampled for paleomagnetism is considered a site, with at least eight samples (cores) collected from each site (flow); one specimen was measured from each sample.

Paleomagnetic samples were analyzed at the UC Berkeley Paleomagnetism Laboratory using a 2G Enterprises DC-SQUID superconducting rock magnetometer, which is within a magnetostatic shield with fields  $\leq 500$  nT (Scott and Frohlich, 1985). The quartz glass sample holder rod used to bring samples into the magnetometer typically has a magnetic moment that is less than  $5 \times 10^{-12}$  Am<sup>2</sup>. After measuring the natural remanent magnetization (NRM), samples were immersed in liquid nitrogen while in a low-field environment ( $<10$  nT) in order to preferentially demagnetize remanence associated with multidomain magnetite by cycling through the Verwey transition and the isotropic point (Verwey, 1939; Feinberg et al., 2015). Samples were then thermally demagnetized through step heating in a magnetically shielded ASC thermal demagnetizing furnace. Following acquisition of thermal demagnetization data, the PmagPy software package (<https://github.com/PmagPy>; Tauxe et al., 2016) was used for principal component analysis of magnetization directions

TABLE 1. U-Pb ZIRCON CA-ID-TIMS DATA

Sample	Th <sup>1</sup> U	Th <sup>1</sup> (x10 <sup>-13</sup> mol)	mol % 206Pb*/206Pb	Pb <sup>§</sup> Pb <sub>c</sub>	Pb <sup>§</sup> (pg)	Radiogenic isotope ratios				Isotopic dates										
						206Pb*/204Pb	206Pb** 206Pb	207Pb** 206Pb	% err <sup>††</sup>	206Pb** 238U	207Pb** 235U	% err <sup>††</sup>	206Pb§§ 238U	207Pb§§ 235U	% err <sup>††</sup>	206Pb§§ 238U				
Sample U1105 (47.0887°N, 95.4504°E)																				
Z1	1.039	1.0663	99.47%	64	0.47	3389	0.326	0.055892	0.161	0.551473	0.214	0.071637	0.080	0.765	445.71	3.58	445.96	0.77	446.01	0.34
Z2	1.706	0.4543	99.01%	40	0.38	1819	0.535	0.055872	0.255	0.552263	0.312	0.071689	0.099	0.684	447.29	5.67	446.48	1.13	446.32	0.43
Z3	1.376	0.1284	96.31%	10	0.41	488	0.432	0.055686	1.033	0.549973	1.126	0.071630	0.217	0.504	439.87	22.99	444.98	4.06	445.97	0.93
Z4	1.059	0.2067	97.82%	15	0.38	826	0.332	0.055658	0.635	0.549821	0.703	0.071645	0.140	0.565	438.77	14.13	444.88	2.53	446.06	0.60
Z5	1.117	0.5249	99.13%	40	0.38	2068	0.350	0.055785	0.266	0.550727	0.319	0.071601	0.096	0.660	443.82	5.91	445.47	1.15	445.79	0.41
Z6	1.058	0.7516	99.35%	53	0.41	2777	0.332	0.055721	0.189	0.551774	0.242	0.071819	0.084	0.738	441.28	4.20	446.16	0.87	447.10	0.36

Note: z1, z2, etc., are labels for analyses composed of single zircon grains that were annealed and chemically abraded (Mattinson, 2005). Labels in bold denote those used in weighted mean calculations.  
 CA-ID-TIMS—chemical abrasion–isotope dilution–thermal ionization mass spectrometry.  
<sup>1</sup>Model Th/U ratio calculated from radiogenic <sup>206</sup>Pb/<sup>206</sup>Pb ratio and <sup>207</sup>Pb/<sup>235</sup>U date.  
<sup>§</sup>Pb\* and Pb<sub>c</sub> are radiogenic and common Pb, respectively, mol % <sup>206</sup>Pb\* is with respect to radiogenic and blank Pb.  
<sup>†</sup>Measured ratio corrected for spike and fractionation only. Fractionation correction is 0.18 ± 0.03 (1σ) %/amu (atomic mass unit) for single-collector. Daly analyses are based on analysis of EARTHTIME <sup>206</sup>Pb-<sup>209</sup>Pb tracer solution.  
<sup>\*\*</sup>Corrected for fractionation, spike, common Pb, and initial disequilibrium in <sup>230</sup>Th/<sup>238</sup>U. Common Pb in analyses was assigned to laboratory blank with a composition of <sup>206</sup>Pb/<sup>204</sup>Pb = 18.04 ± 0.61%, <sup>207</sup>Pb/<sup>204</sup>Pb = 15.54 ± 0.52%, <sup>208</sup>Pb/<sup>206</sup>Pb = 37.69 ± 0.63% (1σ). <sup>206</sup>Pb/<sup>238</sup>U and <sup>207</sup>Pb/<sup>206</sup>Pb ratios were corrected for initial disequilibrium in <sup>230</sup>Th/<sup>238</sup>U using Th/U [magma] = 3.0 ± 0.3 (1σ).  
<sup>††</sup>Errors are 2σ, propagated using algorithms of Schmitz and Schoene (2007) and Crowley et al. (2007).  
<sup>§§</sup>Calculations based on the decay constants of Jaffey et al. (1971). <sup>206</sup>Pb/<sup>238</sup>U and <sup>207</sup>Pb/<sup>235</sup>U using Th/U [magma] = 3.0 ± 0.3 (1σ).

(Kirschvink, 1980). The measurement level data, as well as sample level interpretations, are available in a Github repository associated with this study ([https://github.com/Swanson-Hysell-Group/2016\\_Teel\\_Basalts](https://github.com/Swanson-Hysell-Group/2016_Teel_Basalts)) and as a contribution within the MagIC database (<http://earthref.org/MAGIC/doi/10.1130/L552.1>). Site level interpretations are also available in the **GSA Data Repository**<sup>1</sup>. Examples of specimen demagnetization results are shown in Figure 5. Site means are summarized in Figure 6 and Table 3, with mean calculated poles reported in Table 4.

Three distinct directions were revealed through thermal demagnetization (Fig. 5):

(1) Low-temperature cycling and thermal demagnetization steps to ~150 °C, and sometimes continuing to 300 °C, removed a magnetization for which the direction in geographic coordinates (i.e., no correction for bedding tilt) corresponds to the present local geomagnetic field (Fig. 5). A bootstrap tilt test (Tauxe and Watson, 1994) on these directions revealed the vectors to be significantly better clustered in geographic versus tilt-corrected coordinates. These data therefore fail a tilt test, as expected for a viscous magnetic overprint acquired in recent times (see GSA Data Repository).

(2) Starting as low as 300 °C, and continuing up to the Curie temperature of magnetite (~580 °C), a component was removed in most sites that plots in the upper hemisphere of the southwest quadrant in tilt-corrected coordinates (Figs. 5 and 6). Given the unblocking temperatures over which this component was removed, we interpret it to have been held by (titano)magnetite. Through the stratigraphic succession, there is a progressive decrease in the dip of units (from 58° to 24°). Bedding measurements on thin interflow units of sandstone and siltstone between basalt flows were used for tilt corrections. This decrease in bedding tilt was likely associated with syneruptive tilting during basin development and enables a tilt test to be conducted on the directions from different flows. These directions are better grouped at high levels of untilting than in geographic coordinates, suggesting a pretilting acquisition of remanence (Fig. 6). In the bootstrap tilt test, the best concentration of the data occurs at intermediate levels of untilting, with 95% of the pseudosample maxima lying between 50% and 95% unfolding, and 99% of the pseudosample maxima lying between 39% and 102% unfolding. The small variation in dip between flows throughout the section and the relatively small sample size (N = 23) limit the

<sup>1</sup>GSA Data Repository Item 2016284, a detailed analysis of Teel paleomagnetic data and discussion of the pole compilation, is available at [www.geosociety.org/pubs/ft2016.htm](http://www.geosociety.org/pubs/ft2016.htm), or on request from [editing@geosociety.org](mailto:editing@geosociety.org).

TABLE 2. U-Pb ZIRCON LA-ICP-MS DATA

Analysis	Corrected isotope ratios							Dates (Ma)							
	Th/U	<sup>207</sup> Pb* <sup>235</sup> U*	±2σ (%)	<sup>206</sup> Pb* <sup>238</sup> U	±2σ (%)	Error corr.	<sup>207</sup> Pb* <sup>206</sup> Pb*	±2σ (%)	<sup>207</sup> Pb* <sup>206</sup> Pb*	±2σ (Ma)	<sup>207</sup> Pb* <sup>235</sup> U	±2σ (Ma)	<sup>206</sup> Pb* <sup>238</sup> U*	±2σ (Ma)	% disc.
Sample U1127-5 (46.8786°N, 95.7105°E)															
U1127-5 M 46	0.49	0.33648	5.05	0.04732	3.41	0.67	0.05157	3.72	266	85	294	13	298	10	-12
U1127-5 XL 117	0.77	0.33624	3.08	0.04714	1.75	0.56	0.05173	2.54	274	58	294	8	297	5	-9
U1127-5 M 48	0.59	0.33721	4.19	0.04686	3.81	0.91	0.05219	1.74	294	40	295	11	<b>295</b>	<b>11</b>	-1
U1127-5 XL 112	0.94	0.33112	3.15	0.04652	2.22	0.70	0.05162	2.24	269	51	290	8	<b>293</b>	<b>6</b>	-9
U1127-5 XL 114	0.92	0.32727	3.73	0.04641	2.83	0.76	0.05115	2.43	247	56	287	9	<b>292</b>	<b>8</b>	-18
U1127-5 M 51	0.43	0.33614	4.61	0.04639	3.75	0.81	0.05255	2.69	309	61	294	12	<b>292</b>	<b>11</b>	6
U1127-5 S 151*	0.74	0.32580	5.20	0.04637	4.68	0.90	0.05096	2.25	239	52	286	13	<b>292</b>	<b>13</b>	-22
U1127-5 M 47	0.55	0.33887	5.04	0.04627	4.27	0.85	0.05312	2.67	334	61	296	13	<b>292</b>	<b>12</b>	13
U1127-5 XL 109	0.88	0.32609	3.95	0.04611	1.76	0.44	0.05129	3.53	254	81	287	10	<b>291</b>	<b>5</b>	-14
U1127-5 M 56	0.65	0.33070	5.78	0.04594	5.23	0.90	0.05221	2.45	295	56	290	15	<b>290</b>	<b>15</b>	2
U1127-5 M 44	0.48	0.32480	6.27	0.04587	5.56	0.89	0.05136	2.89	257	67	286	16	<b>289</b>	<b>16</b>	-13
U1127-5 M 53	0.72	0.32941	4.21	0.04587	3.29	0.78	0.05209	2.62	289	60	289	11	<b>289</b>	<b>9</b>	0
U1127-5 S 149	0.46	0.31295	6.22	0.04585	3.90	0.62	0.04951	4.84	172	113	276	15	<b>289</b>	<b>11</b>	-68
U1127-5 XL 113	0.72	0.32736	3.62	0.04579	2.60	0.72	0.05185	2.52	279	58	288	9	<b>289</b>	<b>7</b>	-4
U1127-5 XL 116	0.66	0.32157	4.50	0.04577	3.15	0.70	0.05096	3.22	239	74	283	11	<b>288</b>	<b>9</b>	-21
U1127-5 M 49	0.55	0.32492	4.03	0.04576	3.09	0.77	0.05150	2.58	263	59	286	10	<b>288</b>	<b>9</b>	-10
U1127-5 M 58	0.67	0.32736	4.43	0.04573	3.31	0.75	0.05192	2.94	282	67	288	11	<b>288</b>	<b>9</b>	-2
U1127-5 XL 118	0.77	0.32278	4.22	0.04570	2.33	0.55	0.05122	3.52	251	81	284	10	<b>288</b>	<b>7</b>	-15
U1127-5 M 45	0.93	0.32900	4.63	0.04569	3.99	0.86	0.05222	2.36	295	54	289	12	<b>288</b>	<b>11</b>	2
U1127-5 M 54	0.69	0.32848	4.35	0.04563	3.26	0.75	0.05221	2.88	295	66	288	11	<b>288</b>	<b>9</b>	2
U1127-5 M 50	0.65	0.32826	4.14	0.04558	3.47	0.84	0.05223	2.24	296	51	288	10	<b>287</b>	<b>10</b>	3
U1127-5 S 148*	0.68	0.33023	4.11	0.04550	2.96	0.71	0.05264	2.85	313	65	290	10	<b>287</b>	<b>8</b>	8
U1127-5 XL 107	0.95	0.32381	3.22	0.04544	2.52	0.78	0.05168	2.01	271	46	285	8	<b>286</b>	<b>7</b>	-6
U1127-5 M 55	0.63	0.31321	4.58	0.04540	3.70	0.81	0.05004	2.70	197	63	277	11	<b>286</b>	<b>10</b>	-45
U1127-5 XL 119	0.67	0.31840	2.97	0.04535	2.28	0.76	0.05092	1.91	237	44	281	7	<b>286</b>	<b>6</b>	-21
U1127-5 XL 111	1.40	0.32311	3.98	0.04526	3.71	0.93	0.05177	1.43	275	33	284	10	<b>285</b>	<b>10</b>	-4
U1127-5 XL 110	0.65	0.33080	3.93	0.04510	2.47	0.62	0.05320	3.06	337	69	290	10	<b>284</b>	<b>7</b>	16
U1127-5 XL 108	0.59	0.32377	4.21	0.04506	3.10	0.73	0.05211	2.85	290	65	285	10	<b>284</b>	<b>9</b>	2
U1127-5 M 57	0.49	0.32612	4.43	0.04504	3.42	0.77	0.05252	2.82	308	64	287	11	<b>284</b>	<b>10</b>	8
U1127-5 M 52	0.50	0.32167	7.40	0.04492	6.00	0.81	0.05194	4.32	283	99	283	18	<b>283</b>	<b>17</b>	0
U1127-5 XL 115	0.98	0.32934	2.99	0.04491	1.86	0.62	0.05318	2.34	337	53	289	8	<b>283</b>	<b>5</b>	16
U1127-5 S 147*	0.79	0.31758	4.69	0.04470	4.13	0.87	0.05153	2.21	265	51	280	11	<b>282</b>	<b>11</b>	-7
U1127-5 S 144*	0.61	0.31195	5.60	0.04463	4.57	0.81	0.05069	3.23	227	75	276	14	<b>281</b>	<b>13</b>	-24
U1127-5 S 153*	0.57	0.31941	5.08	0.04462	4.02	0.78	0.05192	3.10	282	71	281	12	<b>281</b>	<b>11</b>	0
U1127-5 S 150*	0.70	0.31131	4.91	0.04456	3.61	0.73	0.05067	3.34	226	77	275	12	<b>281</b>	<b>10</b>	-24
U1127-5 XL 106	0.90	0.31813	2.47	0.04437	1.55	0.62	0.05200	1.92	285	44	280	6	<b>280</b>	<b>4</b>	2
U1127-5 S 145*	0.62	0.32025	4.96	0.04413	4.29	0.86	0.05263	2.50	313	57	282	12	<b>278</b>	<b>12</b>	11
U1127-5 S 143*	0.81	0.29768	5.45	0.04386	4.19	0.76	0.04922	3.48	159	81	265	13	<b>277</b>	<b>11</b>	-75
U1127-5 S 142*	0.64	0.31203	5.01	0.04380	3.60	0.71	0.05167	3.49	271	80	276	12	<b>276</b>	<b>10</b>	-2
U1127-5 S 146*	0.84	0.31108	5.87	0.04375	4.68	0.79	0.05156	3.54	266	81	275	14	<b>276</b>	<b>13</b>	-4
U1127-5 S 154*	1.33	0.30588	6.16	0.04336	5.34	0.86	0.05117	3.06	248	70	271	15	<b>274</b>	<b>14</b>	-10
U1127-5 S 141*	0.93	0.30252	4.82	0.04253	3.79	0.78	0.05159	2.97	267	68	268	11	269	10	-1

Note: Isotope ratio and date errors do not include systematic calibration errors of 0.76% (<sup>207</sup>Pb/<sup>206</sup>Pb) and 1.66% (<sup>206</sup>Pb/<sup>238</sup>U, 2σ). Ablation used a laser spot size of 25 μm and a laser firing repetition rate of 10 Hz. Dates in bold were used for weighted mean date calculation. LA-ICP-MS—laser-ablation—inductively coupled plasma—mass spectrometry. \*Isotope ratio and date errors do not include systematic calibration errors of 0.53% (<sup>207</sup>Pb/<sup>206</sup>Pb) and 1.08% (<sup>206</sup>Pb/<sup>238</sup>U, 2σ).

robustness of the tilt test, and the few flows with directions furthest away from the mean have an oversized impact on the results. Overall, we consider synfolding magnetization unlikely and interpret the distinct improvement in precision upon tilt correction to indicate that the magnetite-held direction is a pretilting primary thermoremanent magnetization (TRM) acquired at the time of eruption and cooling (Fig. 5).

(3) For some sites, there was no remanent magnetization after removal of the magnetite component (e.g., Figs. 5A and B). However, in

many lava flows, samples had remanence that unblocked through temperatures characteristic of hematite (~610–680 °C; Figs. 5C–5F). The magnetization directions associated with this remanence are well grouped as low-inclination south-directed vectors (Fig. 6). In five flows, this same direction was also removed at lower unblocking temperatures within the magnetite range (e.g., Fig. 5F). All hematite directions were near the strike orientation of the bedding and as a result were minimally affected by the applied tilt correction (Fig. 6). As a result, the tilt

test conducted on the population of fits made to hematite-held remanences is ambiguous, with no dominant population of pseudosample maxima, and consequently the test is statistically insignificant (Fig. 6). These results allow for remanence acquisition before or after folding, although the precision of the mean direction is higher in geographic coordinates. Given the distinct direction of the hematite remanence compared to that of magnetite, and also the fact that this southerly and horizontal remanence is dominantly held by hematite, we consider this component to be

Kilian\_L552 1st pages / 8 of 17



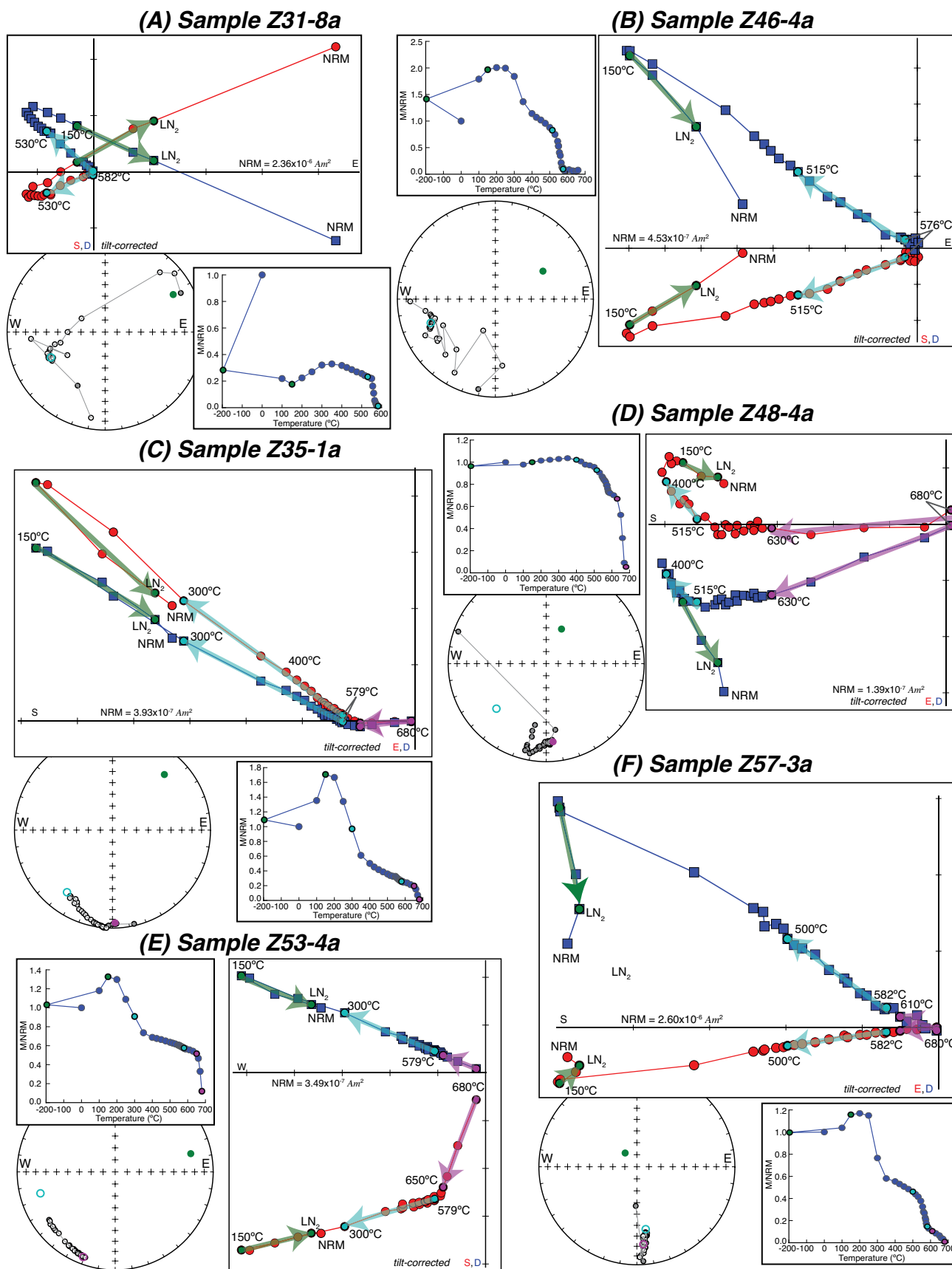


Figure 5.

Figure 5. Demagnetization behavior and vector fits for Teel basalt paleomagnetic samples shown on vector component diagrams, equal-area plots, and plots of normalized intensity. Samples from flows that carry only a magnetite remanence (A–B, blue arrows are magnetite fits) at high temperatures are displayed along with flows that also contain a hematite remanence (C–F, purple arrows are hematite fits). Green arrows indicate least-square fits of remanence held at low temperatures and directed toward the present local field. NRM—natural remanent magnetization.

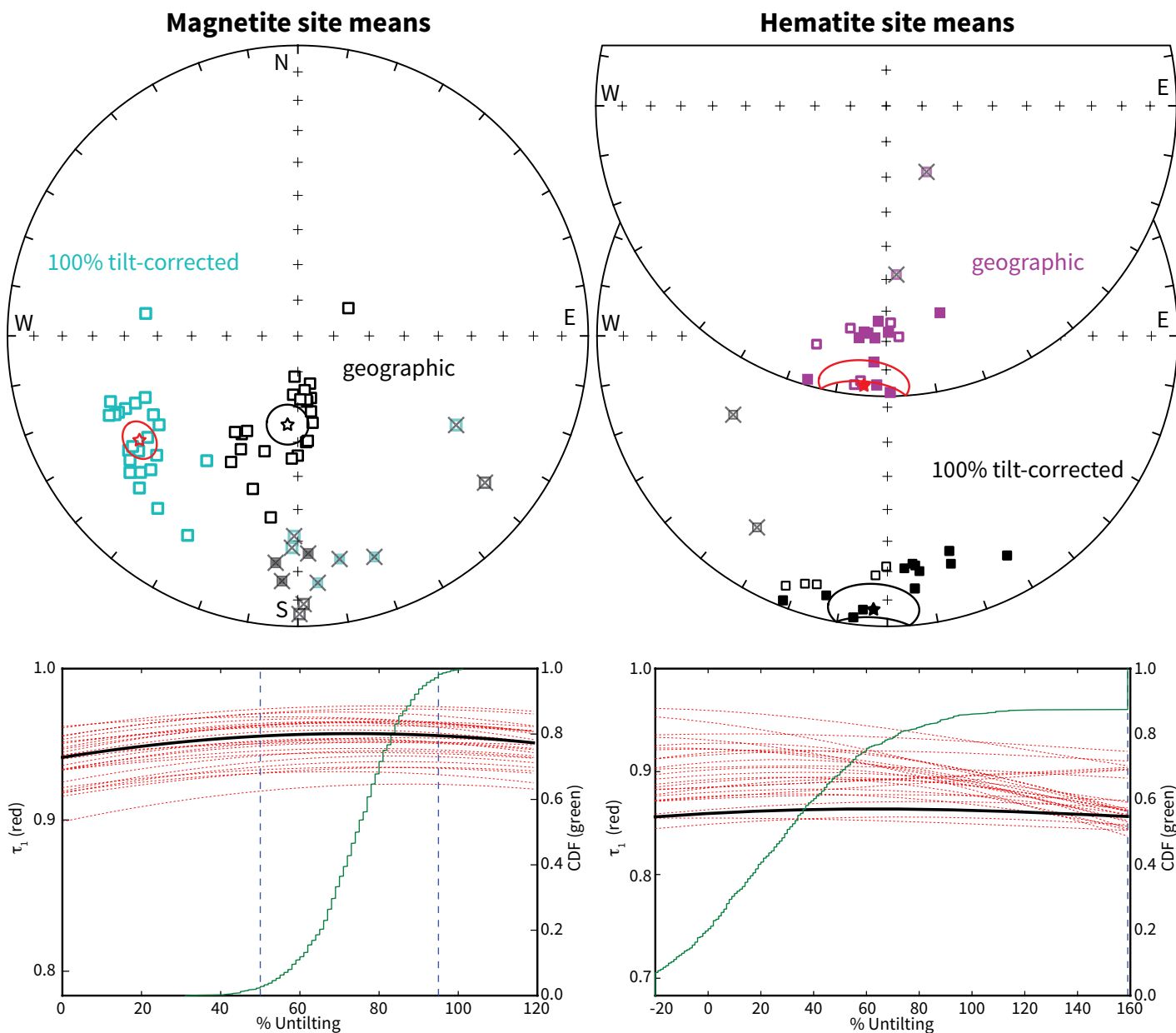


Figure 6. Site means for the magnetite and hematite components of the Teel lava flows shown in both geographic and tilt-corrected coordinates along with the results of bootstrap tilt tests (method of Tauxe and Watson, 1994). The magnitudes of the largest eigenvalue ( $\tau_1$ ) of the orientation matrix with progressive unfolding are shown with the red dashed lines for 25 bootstrapped resamples of the data. For the magnetite component, this eigenvalue is significantly larger at high degrees of untilting than for the in situ data. Due to the similarity between the bedding strike and the remanence directions of the hematite component, the directions of that component, and thereby the concentration of the data set, change little with untilting. As a result, the hematite tilt test is inconclusive. This feature of the data also results in the mean direction being statistically indistinguishable (see Data Repository material) in geographic versus tilt-corrected coordinates. CDF—cumulative distribution function of  $\tau_1$  maxima.

TABLE 3. PALEOMAGNETIC RESULTS FROM THE TEEL FORMATION

	Site_Lat (°N)	Site_Lon (°E)	Dec_geo (°)	Inc_geo (°)	Dec_tc (°)	Inc_tc (°)	$\alpha_{95}$ (°)	<i>n</i>	<i>k</i>	VGP_Lat (°N)	VGP_Lon (°E)
Z30_mag	47.10038	95.3755	61.2	-73.9	278.4	-46.0	11.7	7	27.5	14.4	160.5
Z31_mag	47.10049	95.37604	168.1	-72.2	246.9	-33.3	3.8	8	218.7	28.8	189.3
Z32_mag	47.10094	95.37684	170.4	-65.2	234.1	-32.9	8.0	9	42.4	37.2	199.9
Z33_mag	47.10107	95.37705	184.6	-78.6	250.7	-32.2	4.6	8	147.1	25.8	187.1
Z34_mag	47.10111	95.37712	165.7	-76.2	247.1	-35.8	2.8	10	289.3	29.8	187.8
Z35_mag	47.10069	95.37747	180.0	-56.1	226.2	-25.3	6.4	6	110.6	38.9	211.0
Z36_mag	47.10221	95.37959	184.6	-73.5	247.5	-39.3	4.2	8	177.4	31.2	185.5
Z37_mag	47.10211	95.37971	172.8	-74.7	248.1	-42.7	7.5	9	48.4	32.6	182.9
Z38_mag	47.09855	95.38445	170.1	-68.5	237.4	-42.7	8.0	10	37.2	39.8	190.9
Z39_mag	47.0986	95.38467	196.1	-56.0	230.9	-26.4	6.4	6	111.8	36.4	206.1
Z40_mag	47.09859	95.38474	171.9	-71.4	241.4	-42.8	4.8	9	114.9	37.1	187.7
Z41_mag	47.10109	95.37744	175.5	-59.9	229.1	-29.1	4.6	8	146.6	38.7	206.4
Z42_mag	47.09577	95.38577	196.4	-44.3	219.1	-24.5	11.2	8	25.6	42.7	218.6
Z43_mag	47.0957	95.38638	188.5	-36.9	208.9	-22.6	10.8	8	27.5	47.1	231.3
Z44_mag*	47.09571	95.38651	177.3	26.0	160.9	20.6	12.3	5	39.4	29.8	297.1
Z45_mag*	47.09562	95.38676	185.6	22.6	169.4	22.9	8.3	8	45.5	30.2	287.4
Z46_mag	47.09563	95.38692	209.8	-58.0	235.9	-30.3	6.7	8	68.8	34.9	199.7
Z47_mag	47.09568	95.38727	208.1	-59.6	236.2	-32.1	5.6	8	98.6	35.5	198.5
Z48_mag	47.0957	95.38744	207.9	-49.3	227.7	-32.1	6.8	8	67.9	41.0	206.1
Z49_mag	47.09581	95.38747	213.2	-57.5	236.0	-37.6	9.5	7	41.5	38.2	195.5
Z50_mag*	47.09575	95.38781	183.7	16.5	175.4	15.8	3.9	8	200.4	34.7	280.9
Z51_mag	47.09584	95.38802	206.7	-54.0	229.8	-36.5	10.4	5	55.3	41.8	201.5
Z52_mag	47.09583	95.38815	182.8	-55.2	216.1	-45.8	12.7	6	28.8	55.5	207.7
Z53_mag	47.09442	95.37205	172.3	-72.0	246.7	-32.0	3.6	8	237.8	28.4	190.2
Z54_mag	47.09502	95.37299	177.8	-72.2	247.3	-30.4	4.2	7	204.0	27.3	190.5
Z55_mag	47.09525	95.37351	174.6	-60.3	233.5	-29.0	6.7	8	69.4	35.9	202.4
Z56_mag*	47.06403	95.42075	179.7	-4.8	181.6	-27.9	5.1	6	175.6	57.7	272.5
Z57_mag*	47.06277	95.42039	178.8	-8.5	181.1	-31.6	13.1	6	27.2	60.0	273.4
Z58_mag*	47.06277	95.42045	128.2	-19.4	119.4	-37.6	17.6	6	15.5	35.1	359.0
Z30_hem*		148.8	148.8	-68.2	242.9	-40.2	49.9	7	2.4	69.4	28.8
Z35_hem		185.4	185.4	-5.6	185.1	6.0	5.7	6	137.8	45.4	267.7
Z39_hem		196.3	196.3	-15.6	201.5	2.4	8.7	5	79.0	48.5	250.6
Z40_hem		189.2	189.2	-23.5	202.2	-7.9	7.8	7	61.0	54.3	259.9
Z41_hem		178.8	178.8	-26.2	198.4	-11.1	16.1	5	23.5	56.7	277.4
Z42_hem		165.4	165.4	27.3	151.4	15.0	16.4	6	17.7	27.1	291.2
Z43_hem		182.8	182.8	12.7	173.8	13.6	6.2	8	80.1	36.4	272.0
Z44_hem		182.1	182.1	26.7	163.9	24.0	2.0	7	882.2	28.8	273.0
Z45_hem		179.4	179.4	23.1	164.4	19.7	4.7	8	141.9	30.9	276.0
Z47_hem		186.5	186.5	-3.8	186.9	2.7	14.4	7	18.5	44.5	266.2
Z48_hem		186.7	186.7	20.7	175.8	20.9	5.3	8	112.0	31.9	267.7
Z49_hem		196.0	196.0	2.3	193.3	9.1	17.0	7	13.5	39.7	254.3
Z50_hem		185.6	185.6	22.8	173.7	22.2	3.7	8	225.2	30.8	269.0
Z51_hem		184.6	184.6	22.6	173.1	21.5	10.9	5	50.0	31.0	270.1
Z52_hem		182.8	182.8	21.1	172.2	19.4	13.1	6	27.1	31.9	272.2
Z53_hem		176.9	176.9	-21.5	195.9	-12.1	5.8	7	111.0	53.9	280.6
Z54_hem*		176.6	176.6	-41.3	214.2	-21.4	63.3	7	1.9	66.5	283.3
Z56_hem		179.2	179.2	1.5	180.3	-21.7	8.6	6	61.8	42.2	276.5
Z57_hem		181.9	181.9	4.3	182.8	-18.6	7.5	4	152.6	40.7	272.9

Note: Suffix indicates whether tilt-corrected (\_tc) or geographic (\_geo) directions were used. Site means that are italicized and have an asterisk were not included in the magnetite or hematite mean pole calculation. Magnetite site means were not used if they corresponded with the direction of the hematite population. Hematite site means with  $\alpha_{95} > 20$  were excluded. Magnetite virtual geomagnetic poles (VGPs) were calculated from tilt-corrected data; hematite VGPs were calculated from in situ data. See text for further explanation. *n*—number of samples used for site mean calculation, *k*—Fisher concentration parameter for the site mean distribution, and  $\alpha_{95}$ —radius of 95% confidence interval around site mean direction.

TABLE 4. PALEOMAGNETIC POLES CALCULATED FOR THE TEEL FORMATION

Paleomagnetic pole	Pole_Lat (°N)	Pole_Long (°E)	$A_{95}$ (°)	K	N (sites)	Paleolat. (°N)
Teel_magnetite_tc	36.4	196.2	5.3	33.5	23	19.1
Teel_magnetite_geo	85.8	162.3	8.1	14.9	23	46.6
Teel_hematite_tc	39.6	274.1	7.3	24.7	17	3.2
Teel_hematite_geo	40.0	270.8	5.4	45.4	17	2.7

Note: Suffix on pole name indicates whether tilt-corrected (\_tc) or geographic (\_geo) directions were used.  $A_{95}$ —radius of 95% confidence interval around paleomagnetic pole, K—Fisher concentration parameter for the paleomagnetic pole, and N—number of site mean directions used for calculating the paleomagnetic pole.

secondary and acquired as a chemical remanent magnetization (CRM) sometime after the eruption of the succession and most likely related to the emplacement of the  $286 \pm 5$  Ma Tonkhil Complex. However, given the inconclusive tilt test and lack of a direct geochronologic link, the hematite remanence may have been acquired in middle to late Paleozoic times.

Petrography reveals that samples dominated by magnetite remanence are very well preserved, whereas samples with appreciable hematite remanence have undergone variable degrees of oxidative alteration. Figure 3 shows petrographic photomicrographs for samples for which paleomagnetic data are shown in Figure 5. For example, sample Z31 has a strong magnetite remanence and no indication of hematite remanence (Fig. 5A), and in thin section, the plagioclase, pyroxene, and Fe-Ti oxides are all well preserved. In contrast, sample Z53-4 has a remanence that is dominated by magnetite with some hematite (Fig. 5C), and there is evidence of secondary hematite formation at outcrop and microscopic scale (Figs. 3D, 3E, and 3F). The petrography is consistent with the interpretation that the magnetite remanence is a TRM, and the hematite remanence is a subsequently acquired CRM.

The demagnetization behavior and resulting remanences through magnetite and hematite unblocking temperatures from six sites (three in the northern outcrop and three in the southern) were different from all other sites. Flows Z44, Z45, Z50, Z56, and Z57 all contained one remanence direction oriented to the south and removed through unblocking temperatures characteristic of both magnetite and hematite (Fig. 5F); the hematite remanence typically dominated. If we consider the hematite as secondary, then remanence removed at lower demagnetization temperatures in these flows with the same direction likely resulted from alteration during the fluid flow that produced the hematite. Vertical-axis rotations cannot account for this variation, given that flows immediately above and below contain magnetite remanences that point southeast. Flows Z44, Z45, and Z50 were likely more susceptible to alteration given their mineralogy, and we consider them to be remagnetized. Sites Z56, Z57, and Z58 are from a small section (N1404; Fig. 2) of flows ~7 km to the ESE of all other sites (N1402 and N1403; Fig. 2) with no clear correlation between the outcrop panels. The tilt correction used for this outcrop was measured from flow banding rather than interbedded sedimentary units, making the tilt-corrected data for Z56, Z57, and Z58 unreliable. These flows are also much closer to late Paleozoic intrusions, including the Tonkhil Complex (Fig. 2). Therefore the hematite remanence, which we interpret as secondary, is the

only constraint that can be taken from these basalt flows.

## DISCUSSION

### Age of Paleomagnetic Directions

In the results, we interpreted the magnetite-held remanence direction as being acquired as a thermal remanence when the basalt flows erupted on the basis of the increase in precision upon tilt correction and the excellent preservation of flows in which the remanence was dominated by magnetite (with primary igneous textures including magnetite grains; Figs. 3A and 3I). This interpretation places the age of the tilt-corrected magnetite pole (Table 4) as being the age of the Teel Basalts (ca.  $446.03 \pm 0.21$  Ma). The tilt-corrected mean of the magnetite remanence is unique when compared to available Paleozoic paleomagnetic data from the nearby Mongolian terranes. The magnetite mean is similar to the mid-temperature overprint direction found in Ediacaran to Cambrian rocks from the Zavkhan terrane, both in geographic (in situ) coordinates (Kravchinsky et al., 2001); however, the precision of the Kravchinsky et al. (2001) data increases significantly after tilt correction, suggesting that the geographic direction and its similarity to the Teel magnetite mean is coincidental. Cretaceous results (of reversed polarity) from Mongolia (van Hinsbergen et al., 2008) are also similar in direction to the Teel magnetite geographic mean; however, a Cretaceous remagnetization event that fully overprinted magnetite while leaving the hematite untouched at a distinct direction seems improbable given the primary igneous texture of the magnetite grains with secondary growth of hematite.

The statistically insignificant tilt test for the hematite mean direction makes it difficult to constrain the age of the remanence as post- or pre-folding, enlarging the possible range of acquisition ages. However, because the hematite mean direction is identical in both geographic and tilt-corrected coordinates (see common mean bootstrap test in the Data Repository), we are confident that it accurately portrays an equatorial position of the Zavkhan terrane when the overprint was acquired. In the region, there is evidence for Silurian granites, Permian granites, and deformation that postdate the Silurian granites and predate the Permian ones (Bold et al., 2016). Each of these events could have been associated with the observed secondary hematite. The hematite remanence is similar in direction to existing late Paleozoic paleomagnetic data from Mongolia, including the “B component” of Edel et al. (2014) from the Gobi-Altai terrane, which was likely associated with the

Tuva-Mongolia, Zavkhan, Baidrag, and Lake terranes since Cambrian times (within red dotted outline in Fig. 1B). Edel et al. (2014) incorporated data from Didenko (1992) that are from the Trans-Altai and South Gobi zones (southern terranes), which were sutured to the Central Mongolian terranes by ca. 280 Ma. Although many lack high-precision radiometric ages or robust field tests, other Paleozoic poles that post-date the Ordovician Period across the terranes imply low paleolatitudes similar to that of the Teel hematite remanence (Fig. 7). Some of these paleomagnetic directions, such as equivalent directions reported by Grishin et al. (1991) and Pechersky and Didenko (1995) from Devonian rocks, may have been reset during late Paleozoic or early Mesozoic metamorphism in the southern terranes, as indicated by recent data from the region (Edel et al., 2014; Lehmann et al., 2010; plot included in Data Repository). Taken together, we interpret the hematite remanence, and other constraints, to indicate a low-latitude position for Mongolian terranes sometime following the Ordovician Period and prior to the Mesozoic Era, when they were in mid- to high-latitude positions (Fig. 7).

### Paleontological Considerations

Previous tectonic reviews have cited paleontological data to support an affiliation between the “peri-Siberian” terranes and Siberia throughout the Paleozoic Era (e.g., Cocks and Torsvik, 2007; Wilhem et al., 2012). In contrast, the paleogeographic model described in the next section, which seeks to satisfy the paleomagnetic constraints, predicts that the Zavkhan terrane was situated near Siberia from Cambrian Series 3 to the Late Ordovician Epoch, departed in the Silurian Period, and then returned in the Mesozoic Era. The Paleozoic associations that previous reviews have pointed to are from Cambrian trilobites (e.g., Atashkin et al., 1995; Korobov, 1980, 1989) and Ordovician to Silurian brachiopods (Wang et al., 2011). Although no trilobites have been described from the Zavkhan terrane, early Cambrian trilobites from the associated Tuva-Mongolia terrane are distinct from Siberian trilobites and from those of “peri-Siberian” terranes to the northwest, such as the Altai-Sayan and Gorny-Altai terranes (Atashkin et al., 1995; Korobov, 1980, 1989). The presence of Ordovician to Silurian corals and the low-diversity Silurian *Tuvaella* brachiopods in Mongolia are consistent with a late Cambrian to Silurian connection with Siberia (Ulitina et al., 2009); however, although the distinctive *Tuvaella* brachiopod is found throughout southern and northeastern Mongolia and terranes to the northeast, it is not present on the Siberian

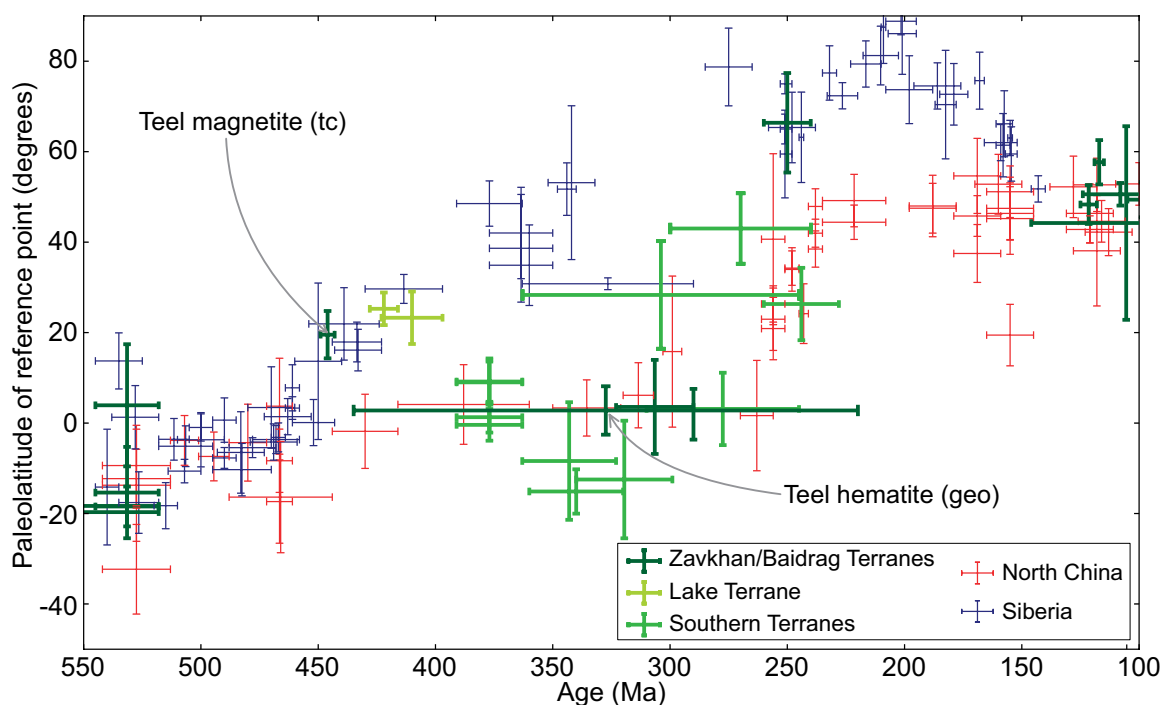


**Figure 7.** Paleolatitude vs. time calculated for reference locations on each terrane: the southern margin of Siberia (present-day 51.7°N, 103.5°E; blue), the northern margin of North China (present-day 42.0°N, 109.0°E; red), and the Zavkhan terrane of Mongolia (present-day 47.1°N, 95.4°E; green). We consider the Zavkhan, Baidrag, and Lake terranes as conjoined since the Cambrian Period. The distinct shades of green correspond to terrane groupings of Mongolia, with the southern terranes including the Khovd, Tsagaanshiviet, Tseel, and Mandal-Ovoo terranes. The magnetite pole from the Teel Formation is shown as  $446 \pm 3$  Ma, while the hematite pole is shown with a large age uncertainty given that it postdates the eruptive age and predates the high-latitude position of the Zavkhan terrane upon closure of the Mongol-Okhotsk Ocean (Van der Voo et al., 2015). The paleolatitude for the geographic hematite direction is shown and is statistically indistinguishable from the tilt-corrected hematite direction (Table 4; see Data Repository). The paleolatitude implied by the hematite component is more compatible with the paleolatitude of North China from the Devonian to Permian Period, which we interpret as the most likely age. All data used in this figure are referenced in the Data Repository.

craton sensu stricto (Wang et al., 2011). After the Ordovician Period, brachiopod assemblages from the Central Mongolian terranes and Siberia diverge (Harper et al., 2013), with Lower and Middle Devonian brachiopods in the Mongolian terranes that constitute Amuria differing from those occurring in Siberia, North China, and South China (Alekseeva et al., 2001; Hou and Boucot, 1990; Boucot and Blodgett, 2001). Webster and Ariunchimeg (2004) described Devonian crinoids in southern Mongolia to be most similar to European and North American fauna. These data, taken together with the geological (Bold et al., 2016) and paleomagnetic data, are consistent with a model in which Late Ordovician to Silurian rifting led to the departure of the Zavkhan terrane (and Lake, Tuva-Mongolia, and Baidrag terranes) from Siberia.

### Paleogeographic Model

The contrasting paleogeographic histories of Siberia and North China throughout the majority of the Paleozoic Era enable us to evaluate

the paleogeographic position of Mongolian terranes relative to these cratons. Figure 7 shows a compilation of paleomagnetic data for Siberia (Cocks and Torsvik, 2007; Powerman et al., 2013; Kravchinsky et al., 2002; Kamysheva, 1971, 1975; Zhitkov et al., 1994; Davydov and Kravchinsky, 1973), North China (Van der Voo et al., 2015; Huang et al., 1999, 2001; Embleton et al., 1996; Doh and Piper, 1994), and the terranes associated with the Zavkhan terrane that coalesced to form Amuria (additional details and references can be found in the Data Repository). Paleomagnetic data coverage for both Siberia and North China is good throughout most of the Paleozoic and Mesozoic Eras, although there are some portions, such as Silurian and Carboniferous times, where gaps arise (Fig. 7). One approach that has been taken to determine the age of poles from Mongolian terranes that are presumed to be peri-Siberian is to date them through comparison to Siberia's apparent polar wander path. This method contrasts with our overarching goal of deducing the cratonic neighbor(s) of the Mongolian terranes during

the Paleozoic Era without a built-in assumption about the connection. In the compilation in Figure 7, we seek to assign ages to poles based on paleontological or radioisotopic constraints.

Our preferred model (Fig. 8), animated using GPlates (animation included in Data Repository), was built primarily using the rotation parameters provided by Domeier and Torsvik (2014) and Domeier (2016) for the 420–250 Ma and 500–420 Ma intervals, respectively. The reconstructions from 250 Ma to the present are based on Euler poles given in Torsvik et al. (2012). The majority of large blocks are positioned according to Torsvik et al. (2012, 2014), with the location and paleolatitude of South China and Annamia (Indochina) approximated using data from Cocks and Torsvik (2013) and modified in consideration of additional paleomagnetic data and studies that indicate a close association with northwest Australia and terranes that originated from it (Han et al., 2015; Jing et al., 2015; Zhang et al., 2015). The position of Tarim in the reconstruction is constrained by poles compiled in Zhao et al. (2014), but it should be considered

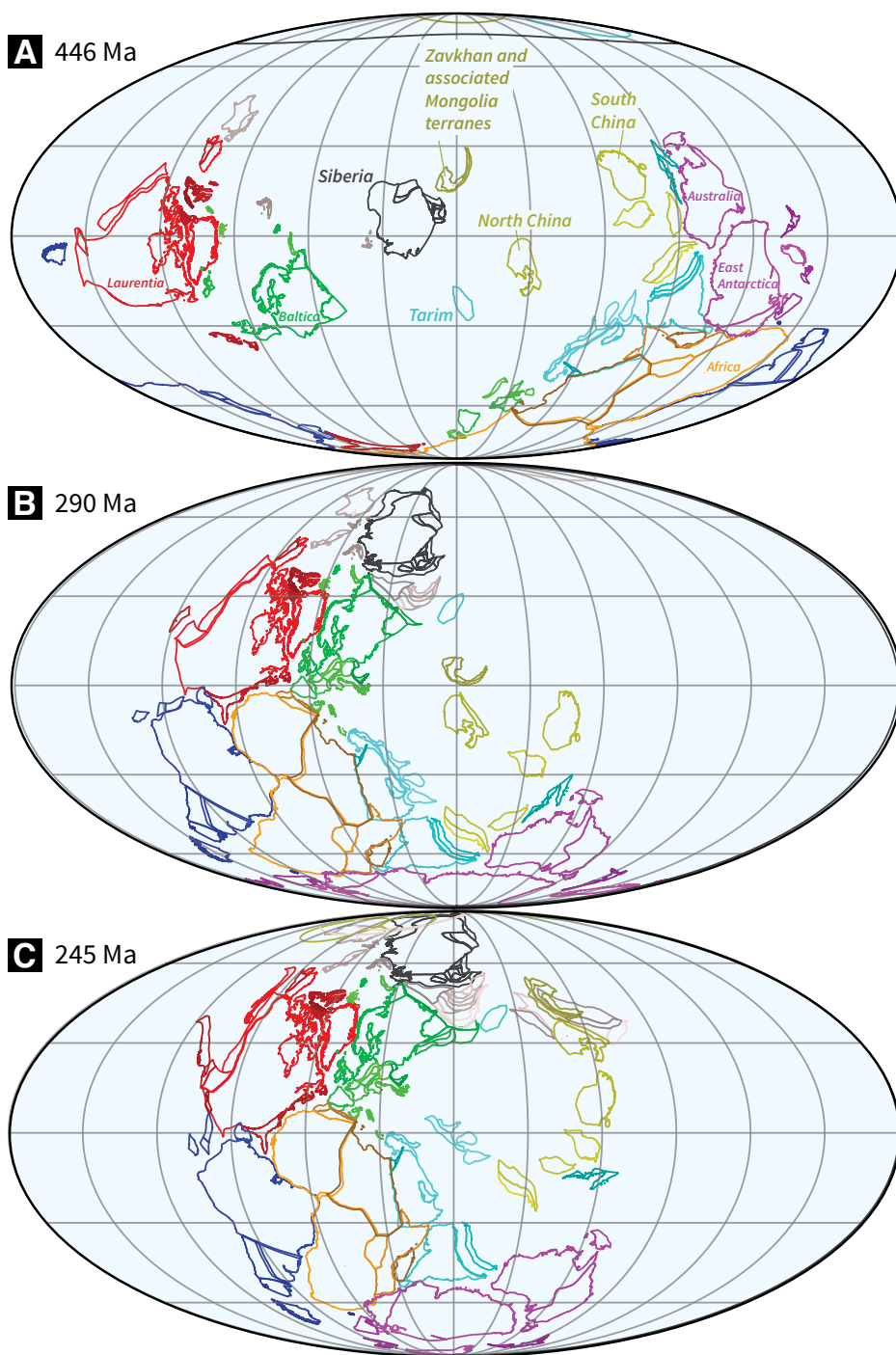


**Figure 8.** Global paleogeographic reconstructions (modified from Domeier and Torsvik, 2014; Domeier, 2016; Torsvik et al., 2012) for three different time periods that highlight the tectonic history of the Central Mongolia terranes, Siberia, and North China. (A) We interpret eruption and deposition of the Teel Formation as coincident with rifting away from Siberia during the Late Ordovician Epoch (see text; Bold et al., 2016). (B) Proximal, equatorial locations are shown for North China and the Central Mongolian terranes during the Permian Period, when the Teel Formation was likely overprinted during the intrusion of granitic plutons. (C) Position of terranes prior to proposed closure of the Mongol-Okhotsk Ocean. Paleomagnetic poles are shown reconstructed to the north pole.

preliminary given the paucity of data. Additional data from Siberia, North China, and the Mongolian terranes that form Amuria were used to create Figure 7 (detailed in the Data Repository) and were used to constrain paleolatitudes in Figure 8. Given the eventual suturing between Siberia and North China with the closure of the Mongol-Okhotsk Ocean (Van der Voo et al., 2015), we considered the possibility that the Zavkhan terrane was associated with North China before suturing, perhaps as early as the Devonian Period. The shape of the Zavkhan and associated terranes used throughout the reconstructions is that of the present day (Fig. 8). This approach is a gross simplification of the history of the terranes, which have undergone oroclinal bending. The history of oroclinal bending and its reconstruction necessitate further work in this portion of the Central Asian orogenic belt. Our approach, at present, is to keep the shape as is and seek to satisfy the paleolatitudinal constraints.

The paleolatitude of the ca. 446 Ma Zavkhan terrane was  $19 \pm 5^\circ \text{N}$  as constrained by the tilt-corrected magnetite component of the Teel Formation basalts and is consistent with it being associated with the Siberia craton in the Late Ordovician Epoch (Fig. 7). Ideally, the consistent polarity of the Teel Formation magnetite remanence could be used to provide a hemisphere constraint. However, the global polarity time scale is poorly constrained for Late Ordovician rocks (Pavlov and Gallet, 2005), allowing for the Teel Formation magnetite remanence (TRM) to have been acquired during a period of either normal or reversed polarity. If the geomagnetic field was of normal polarity (as was interpreted by Pavlov and Gallet [2005] on the basis of data from Khramov et al. [1965]), the Zavkhan terrane must have been in the Southern Hemisphere. A Southern Hemisphere position is inconsistent with early Paleozoic paleontological ties with the present-day southern margin of Siberia (see Paleontological Considerations sections) and could point to an association with Gondwana. However, there is only one study that generated normal polarity data from the Late Ordovician Epoch (Khramov et al., 1965), and it is unclear if these rocks are all older than the Hirnantian Stage. Therefore, we do not consider the global polarity time scale for the interval, as it currently stands, to be a useful tool in determining the polarity of the Teel Formation magnetite remanence.

If the geomagnetic field was of reversed polarity at the time of eruption, the Zavkhan terrane could have been in the Northern Hemisphere and near the present-day southern Siberia margin (Fig. 8A). A similar geologic history potentially links the Zavkhan terrane with the southern Siberian margin from ca. 510 to 450 Ma, when the southwestern margin of the

Zavkhan and Lake terranes may have accreted to southern Siberia (Bold et al., 2016). Beginning in the Ordovician Period, both southern Siberia and the Zavkhan and Lake terranes hosted rift-related extensional magmatism (Dobretsov and Bulsov, 2007; Yarmolyuk, 2011; Cocks and Torsvik, 2007; Bold et al., 2016), including the volcanics of the Teel Formation.

Due to the low paleolatitude implied by the hematite overprint on the Teel Formation, as well as other compiled data from the associated terranes (Fig. 7), the Zavkhan terrane appears to have not traveled with Siberia through the entirety of the Paleozoic Era. The new paleomagnetic data require a tropical position for the Zavkhan terrane when the chemical remanence (hematite) was acquired, which was likely during the middle to late Paleozoic Era. A low-latitude position is indicated by the data both when they are corrected for bedding tilt and when they are not. In contrast, Siberia appears to have remained in the Northern Hemisphere and traveled to progressively higher latitudes from 440 to 200 Ma, as substantiated by Siberia's relatively well-constrained apparent polar wander path from the Ordovician to Devonian Period (Fig. 7; Cocks and Torsvik, 2007; Torsvik et al., 2012). A continued connection of the Zavkhan terrane with Siberia would have resulted in a continuous position in the Northern Hemisphere with drift to progressively higher latitudes (Fig. 7). Due to this constraint, we prefer a model wherein the Zavkhan terrane rifted off of a landmass, likely Siberia, during or soon after ca. 446 Ma eruption of the Teel Formation basalts in extensional (transtensional) basins. This model is similar to the one in Domeier and Torsvik (2014) showing Amuria and Siberia at similar latitudes at 410 Ma. However, their model maintains a high-latitude position for Amuria throughout the Paleozoic (often times higher than Siberia, e.g.,  $\sim 50^\circ\text{N}$  at 370 and 330 Ma), which conflicts with the Teel hematite paleolatitude constraint and some of the Paleozoic paleomagnetic data from other Mongolian terranes (Fig. 7). Even models that extend a linear arc of Mongolian terranes to the south of Siberia cannot accommodate for the large difference in implied paleolatitude.

The linear distribution of Permian peralkaline and alkali-feldspar granitoids that crosscut terrane boundaries in both Mongolia and Siberia has been argued to be a plume-related tie point between the Zavkhan terrane and Siberia (Jahn et al., 2009); however, the wide distribution of pluton ages and the more sparse, less linear distribution of intrusions in Mongolia allow other possible explanations. Given the different paleolatitudes of Siberia and Mongolia during the Permian Period, we believe it is more likely the granitoids formed along a semicontinuous

subduction zone on the margin of the Mongol-Okhotsk Ocean before its Mesozoic closure, as has been proposed in tectonic models (Zhao et al., 1990, 2013; Edel et al. 2014; Kravchinsky et al., 2002). A consistent scenario is that the Mongol-Okhotsk Ocean likely closed like a pair of scissors, as proposed by Edel et al. (2014) and Van der Voo et al. (2015). In our version of this model (Fig. 8), the Tuva-Mongolia and northern Lake terranes were contiguous with the Zavkhan and Baidrag terranes, forming the composite Amuria ribbon continent (Bold et al., 2016). We propose that the northern margin of the ribbon continent collided with Siberia during the late Paleozoic Era, as suggested by metamorphic dates along the Charysh-Terekta-Ulagan-Sayan suture-shear zone and Main Sayan fault (Glorie et al., 2011; Buslov, 2011). The long axis of the Amuria ribbon continent collided roughly orthogonal to the Siberian margin, driving a secondary orocline (Johnston et al., 2013) to develop between the Khubsugul and Zavkhan terranes. This orocline drove the closure of the Mongol-Okhotsk Ocean, with the southern arm of the orocline rotating  $\sim 180^\circ$  relative to Siberia and with the margin and alkali granites folding in on themselves. Constraints for the onset of oroclinal bending and Mongol-Okhotsk Ocean closure may be provided by a  $325.4 \pm 1.1$  Ma date on suprasubduction ophiolites (Tomurtogoo et al., 2005) that presumably formed during subduction initiation. Final closure of the Mongol-Okhotsk Ocean occurred in the Jurassic Period (Van der Voo et al., 2015). This model further implies that the Central Asian orogenic belt did not build exclusively as a long-lived accretionary margin, but instead was greatly modified through the collision of a ribbon continent that was brought into place and oroclinally buckled during a continent-continent collision involving Siberia and North China.

## CONCLUSIONS

Paleomagnetic data from basalts of the Teel Formation of the Zavkhan terrane provide new constraints on the paleogeographic position of a large composite terrane that comprises much of Mongolia and is a significant component of the Central Asian orogenic belt. The geological and geochronological constraints on this composite terrane significantly increase the northward extent of the Amuria microcontinent. While a remanence interpreted to be primary from the Teel Formation basalt flows is consistent with a peri-Siberian position of the block in the Late Ordovician Epoch, such a position later in the Paleozoic Era is not consistent with the results. Therefore, we favor a tectonic and paleogeographic model wherein the Zavkhan, Baidrag,

Tuva-Mongolia, and Lake terranes were separate from Siberia and traveled to the equator subsequently in the Paleozoic Era as the Amuria block. The Mongol-Okhotsk Ocean closed during the Mesozoic Era. During closure, this composite terrane was sandwiched between the Siberia and North China cratons and oroclinally buckled into its present form, which comprises much of present-day Mongolia.

## ACKNOWLEDGMENTS

This research was funded by a UC Berkeley Esper S. Larsen Research Grant, a Hellman Fellowship, and National Science Foundation Grant EAR-1547434 awarded to Swanson-Hysell. Macdonald thanks the National Aeronautics and Space Administration Astrobiology Institute at Massachusetts Institute of Technology node for support. We thank M. Domeier, D. Pastor-Galán, and A. Weil for reviews that greatly improved this manuscript. Odbayar Erdenebat and Ariunsanaa Dorj assisted with field work, and Gunnar Speth assisted with paleomagnetic sample preparation.

## REFERENCES CITED

- Alekseeva, R.E., Afanas'eva, G.A., Shishkina, G.R., and Ushatinskaia, G.T., 2001, Nizhne - i srednedevonskie brachiopody Dal'nego Vostoka Rossii i Mongolii: strofomenidy i khonetidy [Lower and middle Devonian brachiopods of the Far East of Russia and Mongolia: strophomenids and chonetids], Nauka, Moscow, 131 p.
- Atashkin, V.A., Palmer, A.R., Zhuravlev, A.Y., and International Union of Geological Sciences Commission on Stratigraphy Cambrian Correlations Working Group, 1995, The Cambrian system of the foldbelts of Russia and Mongolia: Correlation chart and explanatory notes: Trondheim, Norway, International Union of Geological Sciences, 132 p.
- Badarch, G., Dickson Cunningham, W., and Windley, B.F., 2002, A new terrane subdivision for Mongolia: Implications for the Phanerozoic crustal growth of Central Asia: *Journal of Asian Earth Sciences*, v. 21, no. 1, p. 87-110.
- Bold, U., Crowley, J., Smith, E., Sambuu, O., and Macdonald, F., 2016, Neoproterozoic to early Paleozoic tectonic evolution of the Zavkhan terrane of Mongolia: Implications for crustal growth in the Central Asian orogenic belt: *Lithosphere*, doi:10.1130/L549.1 (in press).
- Boucot, A., and Blodgett, R., 2001, Silurian-Devonian biogeography, in Brunton, H.C., Cocks, R.M., and Long, S.L., eds., *Brachiopods Past and Present*, the Natural History Museum: London, Taylor & Francis Publishers, p. 335-344.
- Buslov, M., 2011, Tectonics and geodynamics of the Central Asian foldbelt: The role of late Paleozoic large-amplitude strike-slip faults: *Russian Geology and Geophysics*, v. 52, no. 1, p. 52-71, doi:10.1016/j.rgg.2010.12.005.
- Byamba, J., 2009, Late Paleozoic to Early Mesozoic structures, in Byamba, J., Badamgarav, J., Bayasgalan, A., Arvisbaatar, N., Turutanov, E. H., Dorjsuren, B., Tomurhuu, D., Dejidmaa, G., Dorjnamjaa, D., Mahbadar, T., and Amarjargal, A., eds., *Geology and Minerals of Mongolia: Lithosphere plate tectonics: Ulaanbaatar, Mongolia, Soyombo Printing*, p. 353-358.
- Cocks, L.R.M., and Torsvik, T.H., 2007, Siberia, the wandering northern terrane, and its changing geography through the Palaeozoic: *Earth-Science Reviews*, v. 82, p. 29-74, doi:10.1016/j.earscirev.2007.02.001.
- Cocks, L.R.M., and Torsvik, T.H., 2013, The dynamic evolution of the Palaeozoic geography of eastern Asia: *Earth-Science Reviews*, v. 117, p. 40-79, doi:10.1016/j.earscirev.2012.12.001.
- Cogné, J.-P., Kravchinsky, V.A., Halim, N., and Hankard, F., 2005, Late Jurassic-Early Cretaceous closure of the Mongol-Okhotsk Ocean demonstrated by new Mesozoic paleomagnetic results from the Trans-Baikal area (SE Siberia): *Geophysical Journal International*, v. 163, p. 813-832, doi:10.1111/j.1365-246X.2005.02782.x.
- Crowley, J.L., Schoene, B., and Bowring, S.A., 2007, U-Pb dating of zircon in the Bishop Tuff at the millennial scale: *Geology*, v. 35, no. 12, p. 1123-1126.

- Davydov, V., and Kravchinsky, A., 1973, Paleomagnetic Directions and Pole Positions: Data for the USSR Issue 2: Moscow, Soviet Geophysical Committee, World Data Center-B, Catalogue.
- Didenko, A.N., 1992, Magnetism of South Mongolian middle Paleozoic ophiolites: Physics of the Earth and Planetary Interiors, v. 74, p. 263–277, doi:10.1016/0031-9201(92)90014-M.
- Dobretsov, N., and Buslov, M., 2007, Late Cambrian–Ordovician tectonics and geodynamics of Central Asia: Russian Geology and Geophysics, v. 48, p. 71–82, doi:10.1016/j.rgg.2006.12.006.
- Doh, S.-J., and Piper, J.D.A., 1994, Palaeomagnetism of the (Upper Palaeozoic–Lower Mesozoic) Pyongan Super-group, Korea: A Phanerozoic link with the North China block: Geophysical Journal International, v. 117, p. 850–863, doi:10.1111/j.1365-246X.1994.tb02475.x.
- Domeier, M., 2016, A plate tectonic scenario for the Iapetus and Rheic Oceans: Gondwana Research, v. 36, p. 275–295, doi:10.1016/j.jgr.2015.08.003.
- Domeier, M., and Torsvik, T.H., 2014, Plate tectonics in the late Paleozoic: Geoscience Frontiers, v. 5, p. 303–350, doi:10.1016/j.gsf.2014.01.002.
- Edel, J.B., Schulmann, K., Hanzl, P., and Lexa, O., 2014, Palaeomagnetic and structural constraints on 90° anticlockwise rotation in SW Mongolia during the Permo-Triassic: Implications for Altaid oroclinal bending. Preliminary palaeomagnetic results: Journal of Asian Earth Sciences, v. 94, p. 157–171, doi:10.1016/j.jseaes.2014.07.039.
- Embleton, B.J.J., McElhinny, M.W., Ma, X., Zhang, Z., and Xiang Li, Z., 1996, Permo-Triassic magnetostratigraphy in China: The type section near Taiyuan, Shanxi Province, North China: Geophysical Journal International, v. 126, p. 382–388, doi:10.1111/j.1365-246X.1996.tb05298.x.
- Feinberg, J., Solheid, P., Swanson-Hysell, N., Jackson, M., and Bowles, J., 2015, Full vector low-temperature magnetic measurements of geologic materials: Geochemistry, Geophysics, Geosystems, v. 16, p. 301–314, doi:10.1002/2014GC005591.
- Gibson, T., Myrow, P., Macdonald, F., Minjin, C., and Gehrels, G., 2013, Depositional history, tectonics, and detrital zircon geochronology of Ordovician and Devonian strata in southwestern Mongolia: Geological Society of America Bulletin, v. 125, p. 877–893, doi:10.1130/B30746.1.
- Glorie, S., De Grave, J., Buslov, M., Zhimulev, F., Izmer, A., Vandorner, W., Ryabinin, A., Vanhaecke, F., and Elburg, M., 2011, Formation and Palaeozoic evolution of the Gornyy Altai–Altai–Mongolia suture zone (South Siberia): Zircon U/Pb constraints on the igneous record: Gondwana Research, v. 20, no. 2, p. 465–484, doi:10.1016/j.gr.2011.03.003.
- Grishin, D., Didenko, A., Pechersky, D., and T.L., T., 1991, Palaeomagnetic study and petromagnetic study of structure and evolution of paleoceanic lithosphere (Phanerozoic ophiolites of Asia), in Khramov A.N., ed., Palaeomagnetism and Paleogeodynamics of the USSR Territory: Leningrad, Russia, VNIIGRI, p. 135–149 [in Russian].
- Han, Z., Yang, Z., Tong, Y., and Jing, X., 2015, New paleomagnetic results from Late Ordovician rocks of the Yangtze block, South China, and their paleogeographic implications: Journal of Geophysical Research–Solid Earth, v. 120, p. 4759–4772, doi:10.1002/2015JB012005.
- Harper, D.A.T., Rasmussen, C.M.Ø., Liljeroth, M., Blodgett, R.B., Candela, Y., Jin, J., Percival, I.G., Rong, J.-Y., Villas, E., and Zhan, R.-B., 2013, Chapter 11, Biodiversity, biogeography and phylogeography of Ordovician rhynchonelliform brachiopods, in Harper, D.A.T., and Servais, T., eds., Early Palaeozoic Biogeography and Palaeogeography: Geological Society, London, Memoir 38, p. 127–144, doi:10.1144/M38.11.
- Hou, H.-F., and Boucot, A.J., 1990, The Balkhash–Mongolia–Okhotsk region of the Old World Realm (Devonian), in McKerron, W.S., and Scotese, C.R., eds., Palaeozoic Palaeogeography and Biogeography: Geological Society, London, Memoir 12, p. 297–303, doi:10.1144/GSL.MEM.1990.012.01.29.
- Huang, B., Yang, Z., Otofuiji, Y., and Zhu, R., 1999, Early Paleozoic paleomagnetic poles from the western part of the North China block and their implications: Tectonophysics, v. 308, p. 377–402, doi:10.1016/S0040-1951(99)00098-0.
- Huang, B., Otofuiji, Y.-I., Zhu, R., Shi, R., and Wang, Y., 2001, Paleomagnetism of Carboniferous sediments in the Hexi corridor: Its origin and tectonic implications: Earth and Planetary Science Letters, v. 194, p. 135–149, doi:10.1016/S0012-821X(01)00557-X.
- Ilyin, A.V., 1990, Proterozoic supercontinent, its latest Precambrian rifting, breakup, dispersal into smaller continents, and subsidence of their margins: Evidence from Asia: Geology, v. 18, p. 1231–1234, doi:10.1130/0091-7613(1990)018<1231:PSILPR>2.3.CO;2.
- Jaffey, A.H., Flynn, K.F., Glendenin, L.E., Bentley, W.C., and Essling, A.M., 1971, Precision measurement of half-lives and specific activities of <sup>235</sup>U and <sup>238</sup>U: Physical Review C, v. 4, no. 5, p. 1889–1906.
- Jahn, B., Litvinovsky, B., Zarnivlevich, A., and Reichow, M., 2009, Peralkaline granitoid magmatism in the Mongolian-Transbaikalian belt: Evolution, petrogenesis and tectonic significance: Lithos, v. 113, p. 521–539, doi:10.1016/j.lithos.2009.06.015.
- Jian, P., Kröner, A., Jahn, B.-m., Windley, B.F., Shi, Y., Zhang, W., Zhang, F., Miao, L., Tomurhuu, D., and Liu, D., 2014, Zircon dating of Neoproterozoic and Cambrian ophiolites in West Mongolia and implications for the timing of orogenic processes in the central part of the Central Asian orogenic belt: Earth-Science Reviews, v. 133, p. 62–93, doi:10.1016/j.earscirev.2014.02.006.
- Jing, X.-Q., Yang, Z., Tong, Y., and Han, Z., 2015, A revised paleomagnetic pole from the mid-Neoproterozoic Liantuo Formation in the Yangtze block and its paleogeographic implications: Precambrian Research, v. 268, p. 194–211, doi:10.1016/j.precamres.2015.07.007.
- Johnston, S.T., Weil, A., and Gutiérrez-Alonso, G., 2013, Orogenies: Thick and thin: Geological Society of America Bulletin, v. 125, no. 5–6, p. 643–663, doi:10.1130/B30765.1.
- Kamysheva, G., 1971, Paleomagnetic Directions and Pole Positions: Data for the USSR Issue 1: Moscow, Soviet Geophysical Committee, World Data Center-B, Catalogue.
- Kamysheva, G., 1975, Paleomagnetic Directions and Pole Positions: Data for the USSR Issue 3: Moscow, Soviet Geophysical Committee, World Data Center-B, Catalogue.
- Khain, E., Bibikova, E., Salnikova, E., Kröner, A., Gibsher, A., Didenko, A., Degtyarev, K., and Fedotova, A., 2003, The palaeo-Asian Ocean in the Neoproterozoic and early Palaeozoic: New geochronologic data and palaeotectonic reconstructions: Precambrian Research, v. 122, p. 329–358, doi:10.1016/S0301-9268(02)00218-8.
- Khramov, A., Rodionov, V., and Komissarova, R., 1965, New data on the Paleozoic history of the geomagnetic field in the USSR, in Nastoyashee i proshloe magnitno go polja Zemli (The Present and Past of the Geomagnetic Field) [translated by E.R. Hope, Director of Scientific Information Services, DRB Canada T460R, 1966]: Moscow, Nauka, p. 206–213.
- Kirschvink, J., 1980, The least-squares line and plane and the analysis of paleomagnetic data: Geophysical Journal of the Royal Astronomical Society, v. 62, p. 699–718, doi:10.1111/j.1365-246X.1980.tb02601.x.
- Korobov, M., 1980, Biostratigraphy and miomeric trilobites from the Lower Cambrian of Mongolia: The Joint Soviet-Mongolian Scientific Research Geological Expedition Transactions, v. 26, p. 5–108 [in Russian].
- Korobov, M., 1989, Biostratigraphy and Lower Cambrian Polymeric Trilobites of Mongolia: The Joint Soviet-Mongolian Scientific Research Geological Expedition Transactions, v. 48, p. 1–202 [in Russian].
- Kovalenko, D., 2010, Paleomagnetism of late Paleozoic, Mesozoic, and Cenozoic rocks in Mongolia: Russian Geology and Geophysics, v. 51, p. 387–403, doi:10.1016/j.rgg.2010.03.006.
- Kravchinsky, V., Konstantinov, K., and Conge, J., 2001, Palaeomagnetic study of Vendian and Early Cambrian rocks of South Siberia and Central Mongolia: Was the Siberian platform assembled at this time? Precambrian Research, v. 110, p. 61–92, doi:10.1016/S0301-9268(01)00181-4.
- Kravchinsky, V.A., Cogné, J.-P., Harbert, W.P., and Kuzmin, M.I., 2002, Evolution of the Mongol-Okhotsk Ocean as constrained by new palaeomagnetic data from the Mongol-Okhotsk suture zone, Siberia: Geophysical Journal International, v. 148, p. 34–57, doi:10.1046/j.1365-246X.2002.01557.x.
- Kröner, A., Lehmann, J., Schulmann, K., Demoux, A., Lexa, O., Tomurhuu, D., Štípská, P., Liu, D., and Wingate, M.T.D., 2010, Lithostratigraphic and geochronological constraints on the evolution of the Central Asian orogenic belt in SW Mongolia: Early Paleozoic rifting followed by late Paleozoic accretion: American Journal of Science, v. 310, p. 523–574, doi:10.2475/072010.01.
- Kuzmichev, A.B., Bibikova, E.V., and Zhuravlev, D.Z., 2001, Neoproterozoic (800 Ma) orogeny in the Tuva-Mongolia Massif (Siberia): Island arc-continent collision at the northeast Rodinia margin: Precambrian Research, v. 110, p. 109–126, doi:10.1016/S0301-9268(01)00183-8.
- Lamb, M.A., and Badarch, G., 2001, Paleozoic sedimentary basins and volcanic arc systems of southern Mongolia: New geochemical and petrographic constraints, in Hendrix, M.S., and Davis, G.A., eds., Paleozoic and Mesozoic Tectonic Evolution of Central and Eastern Asia: From Continental Assembly to Intracontinental Deformation: Geological Society of America Memoir 194, p. 117–149, doi:10.1130/0-8137-1194-0.117.
- Lehmann, J., Schulmann, K., Lexa, O., Corsini, M., Kröner, A., Štípská, P., Tomurhuu, D., and Otgonbator, D., 2010, Structural constraints on the evolution of the Central Asian orogenic belt in SW Mongolia: American Journal of Science, v. 310, p. 575–628, doi:10.2475/072010.02.
- Levashova, N.M., Kalugin, V.M., Gibsher, A.S., Yff, J., Ryabinin, A.B., Meert, J.G., and Malone, S.J., 2010, The origin of the Baydaric microcontinent, Mongolia: Constraints from paleomagnetism and geochronology: Tectonophysics, v. 485, p. 306–320, doi:10.1016/j.tecto.2010.01.012.
- Ludwig, K., 2008, User's Manual for Isoplot 3.70: A Geochronological Toolkit for Microsoft Excel: Berkeley Geochronology Center Special Publication 4, 77 p.
- Macdonald, F.A., Jones, D.S., and Schrag, D.P., 2009, Stratigraphic and tectonic implications of a newly discovered glacial diamicite-cap carbonate couplet in southwestern Mongolia: Geology, v. 37, p. 123–126, doi:10.1130/G24797A.1.
- Macdonald, F.A., Ryan-Davis, J., Coish, R.A., Crowley, J.L., and Karabinos, P., 2014, A newly identified Gondwanan terrane in the northern Appalachian Mountains: Implications for the Taconic orogeny and closure of the Iapetus Ocean: Geology, v. 42, p. 539–542, doi:10.1130/G35659.1.
- Mattinson, J.M., 2005, Zircon U/Pb chemical abrasion (CA-TIMS) method: Combined annealing and multistep partial dissolution analysis for improved precision and accuracy of zircon ages: Chemical Geology, v. 220, p. 47–66, doi:10.1016/j.chemgeo.2005.03.011.
- Mossakovsky, A., Ruzhentsev, S., Samygin, S., and Kheraskova, T., 1994, Central Asian fold belt: Geodynamic evolution and formation history: Geotectonics, v. 27, p. 445–474.
- Pavlov, V., and Gallet, Y., 2005, A third superchron during the early Paleozoic: Episodes, v. 28, p. 78–84.
- Pechersky, D., and Didenko, A., 1995, Paleo-Asian Ocean: Moscow, United Institute of Earth's Physics Publishers, 298 p. [in Russian].
- Powerman, V., Shatsillo, A., Coe, R., Zhao, X., Gladkochub, D., Buchwaldt, R., and Pavlov, V., 2013, Palaeogeography of the Siberian platform during middle Paleozoic times (450–400 Ma): New palaeomagnetic evidence from the Lena and Nyuya Rivers: Geophysical Journal International, v. 194, p. 1412–1440, doi:10.1093/gji/ggt197.
- Rojas-Agramonte, Y., Kröner, A., Demoux, A., Xia, X., Wang, W., Donskaya, T., Liu, D., and Sun, M., 2011, Detrital and xenocrystic zircon ages from Neoproterozoic to Palaeozoic arc terranes of Mongolia: Significance for the origin of crustal fragments in the Central Asian orogenic belt: Gondwana Research, v. 19, p. 751–763, doi:10.1016/j.jgr.2010.10.004.
- Schmitz, M.D., and Schoene, B., 2007, Derivation of isotope ratios, errors, and error correlations for U-Pb geochronology using <sup>205</sup>Pb-<sup>235</sup>U-(<sup>233</sup>U)-spiked isotope dilution thermal ionization mass spectrometric data: Geochemistry, Geophysics, Geosystems, v. 8, no. 8, p. 20.
- Scott, G.R., and Frohlich, C., 1985, Large-Volume, Magnetically Shielded Room, in Kirschvink, J.L., Jones, D.S., and MacFadden, B.J., eds., Magnetite Biomineralization and Magnetoreception in Organisms: A New Biomagnetism: Boston, MA, Springer US, p. 197–220.
- Şengör, A., and Natal'in, B.A., 1996, Turkic-type orogeny and its role in the making of the continental crust: Annual Review of Earth and Planetary Sciences, v. 24, p. 263–337, doi:10.1146/annurev.earth.24.1.263.
- Şengör, A., Natal'in, B., and Burtman, V., 1993, Evolution of the Altaid tectonic collage and Paleozoic crustal growth in Eurasia: Nature, v. 364, p. 299–307, doi:10.1038/364299a0.



- Tauxe, L., and Watson, G.S., 1994, The fold test: An eigen analysis approach: *Earth and Planetary Science Letters*, v. 122, no. 3, p. 331–341.
- Tauxe, L., Shaar, R., Jonestrask, L., Swanson-Hysell, N., Minnett, R., Koppers, A., Constable, C., Jarboe, N.A., Gaastra, K., and Fairchild, L., 2016, PmagPy: Software package for paleomagnetic data analysis and a bridge to the Magnetism Information Consortium (MagIC) Database: *Geochemistry, Geophysics, and Geosystems*, v. 17, no. 6, p. 2450–2463, doi:10.1002/2016GC006307.
- Togtokh, D., Baatarkhuyag, A., and Bayardalai, S., 1995, The Report of Result of the Geological Grouped Mapping: Ulaanbaatar, Mongolia, Mineral Resources Authority of Mongolia, scale 1:200,000.
- Tomurtogoo, O., Windley, B., Kröner, A., Badarch, G., and Liu, D., 2005, Zircon age and occurrence of the Aadaat-sag ophiolite and Muron shear zone, central Mongolia: Constraints on the evolution of the Mongol-Okhotsk Ocean, suture and orogen: *Journal of the Geological Society, London*, v. 162, no. 1, p. 125–134, doi:10.1144/0016-764903-146.
- Torsvik, T.H., Van der Voo, R., Preeden, U., Mac Niocaill, C., Steinberger, B., Doubrovine, P.V., van Hinsbergen, D.J.J., Domeier, M., Gaina, C., Tohver, E., Meert, J.G., McCausland, P.J.A., and Cocks, L.R.M., 2012, Phanerozoic polar wander, palaeogeography and dynamics: *Earth-Science Reviews*, v. 114, p. 325–368, doi:10.1016/j.earscirev.2012.06.007.
- Torsvik, T.H., van der Voo, R., Doubrovine, P.V., Burke, K., Steinberger, B., Ashwal, L.D., Trønnes, R.G., Webb, S.J., and Bull, A.L., 2014, Deep mantle structure as a reference frame for movements in and on the Earth: *Proceedings of the National Academy of Sciences of the United States of America*, v. 111, no. 24, p. 8735–8740, doi:10.1073/pnas.1318135111.
- Ulitina, L., Bondarenko, O., and Minjin, C., 2009, Evolution of the taxonomic diversity of Mongolian Ordovician–Silurian corals: *Paleontological Journal*, v. 43, p. 499–505, doi:10.1134/S0031030109050049.
- Van der Voo, R., van Hinsbergen, D.J.J., Domeier, M., Spakman, W., and Torsvik, T.H., 2015, Latest Jurassic–earliest Cretaceous closure of the Mongol-Okhotsk Ocean: A paleomagnetic and seismological tomographic analysis, *in* Anderson, T.H., Didenko, A.N., Johnson, C.L., Khanchuk, A.I., and MacDonald, J.H., Jr., eds., *Late Jurassic Margin of Laurasia—A Record of Faulting Accommodating Plate Rotation*: Geological Society of America Special Paper 513, p. 589–606.
- van Hinsbergen, D.J.J., Straathof, G.B., Kuiper, K.F., Cunningham, W.D., and Wijbrans, J., 2008, No vertical axis rotations during Neogene transpressional orogeny in the NE Gobi Altai: Coinciding Mongolian and Eurasian Early Cretaceous apparent polar wander paths: *Geophysical Journal International*, v. 173, p. 105–126, doi:10.1111/j.1365-246X.2007.03712.x.
- Verwey, E.J.W., 1939, Electronic conduction of magnetite (Fe<sub>3</sub>O<sub>4</sub>) and its transition point at low temperatures: *Nature*, v. 144, p. 327–328, doi:10.1038/144327b0.
- Wang, T., Zheng, Y., Zhang, J., Zeng, L., Donskaya, T., Guo, L., and Li, J., 2011, Pattern and kinematic polarity of late Mesozoic extension in continental NE Asia: Perspectives from metamorphic core complexes: *Tectonics*, v. 30, p. TC6007, doi:10.1029/2011TC002896.
- Webster, G.D., and Ariunchimeg, Y., 2004, The northernmost Emsian crinoids known, a Devonian fauna from the Chuluun Formation, Shine Jinst area, southern Mongolia: *Geobios*, v. 37, p. 481–487, doi:10.1016/j.geobios.2003.07.001.
- Wilhem, C., Windley, B.F., and Stampfli, G.M., 2012, The Altaids of Central Asia: A tectonic and evolutionary innovative review: *Earth-Science Reviews*, v. 113, p. 303–341, doi:10.1016/j.earscirev.2012.04.001.
- Windley, B.F., Alexeev, D., Xiao, W., Kröner, A., and Badarch, G., 2007, Tectonic models for accretion of the Central Asian orogenic belt: *Journal of the Geological Society, London*, v. 164, p. 31–47, doi:10.1144/0016-76492006-022.
- Yakubchuk, A., 2008, Re-deciphering the tectonic jigsaw puzzle of northern Eurasia: *Journal of Asian Earth Sciences*, v. 32, p. 82–101, doi:10.1016/j.jseaes.2007.10.009.
- Yarmolyuk, V., Samoilov, B., and Ivanov, V., 1999, Composition and sources of basalts in the late Paleozoic rift system of Central Asia: Geochemical and isotopic data: *Geochemistry*, v. 10, p. 1027–1042.
- Yarmolyuk, V.V., Kovach, V.P., Kovalenko, V.I., Salnikova, E.B., Kozlovskii, A.M., Kotov, A.B., Yakovleva, S.Z., and Fedosenko, A.M., 2011, Composition, sources, and mechanism of continental crust growth in the Lake zone of the Central Asian Caledonides: I. Geological and geochronological data: *Petrology*, v. 19, no. 1, p. 55–78.
- Zacek, V., Buriánek, D., Pecsckay, Z., and Skoda, R., 2016, Astrophyllite-alkali amphibole rhyolite, an evidence of Early Permian A-type alkaline volcanism in the western Mongolian Altai: *Journal of Geosciences (Prague)*, v. 61, p. 93–103, doi:10.3190/jgeosci.205.
- Zhang, S., Li, H., Jiang, G., Evans, D.A., Dong, J., Wu, H., Yang, T., Liu, P., and Xiao, Q., 2015, New paleomagnetic results from the Ediacaran Doushantuo Formation in South China and their paleogeographic implications: *Precambrian Research*, v. 259, p. 130–142, doi:10.1016/j.precamres.2014.09.018.
- Zhao, P., Chen, Y., Xu, B., Faure, M., Shi, G., and Choulet, F., 2013, Did the paleo-Asian Ocean between the North China block and Mongolia block exist during the late Paleozoic? First paleomagnetic evidence from central-eastern Inner Mongolia, China: *Journal of Geophysical Research—Solid Earth*, v. 118, p. 1873–1894, doi:10.1002/jgrb.50198.
- Zhao, P., Chen, Y., Zhan, S., Xu, B., and Faure, M., 2014, The apparent polar wander path of the Tarim block (NW China) since the Neoproterozoic and its implications for a long-term Tarim–Australia connection: *Precambrian Research*, v. 242, p. 39–57, doi:10.1016/j.precamres.2013.12.009.
- Zhao, X., Coe, R., Zhou, Y., Wu, H., and Wang, J., 1990, Tectonics of eastern Asia and western Pacific continental margin—New paleomagnetic results from northern China: Collision and suturing with Siberia and Kazakhstan: *Tectonophysics*, v. 181, p. 43–81, doi:10.1016/0040-1951(90)90008-V.
- Zhitkov, A., Kravchinsky, V., and Konstantinov, K., 1994, Paleomagnetic Studies Aimed at Obtaining Paleomagnetic Data for the Geodynamics of the Eastern USSR (East of the Enisey River): Report on Theme 01423412334 for 1991–1994: Irkutsk, Geological Committee of Russia [in Russian], 246 p.

MANUSCRIPT RECEIVED 13 APRIL 2015  
 REVISED MANUSCRIPT RECEIVED 11 JULY 2016  
 MANUSCRIPT ACCEPTED 18 AUGUST 2016

Printed in the USA